Scanning tunneling microscopy of the charge-density-wave structure in $1T$-TaS_2

R. E. Thomson*
Department of Physics, University of California, Berkeley, California 94720
and Materials Science Division, Lawrence Berkeley Laboratory, Berkeley, California 94720

B. Burk and A. Zettl
Department of Physics, University of California, Berkeley, California 94720

John Clarke
Department of Physics, University of California, Berkeley, California 94720
and Materials Science Division, Lawrence Berkeley Laboratory, Berkeley, California 94720
(Received 21 June 1993; revised manuscript received 15 February 1994)

Using scanning tunneling microscopy (STM), we studied $1T$-TaS_2 in all four of its charge-density-wave (CDW) supporting phases over the temperature range 360–143 K. Special attention was given to the search for discommensurate structures and the distinguishing of true CDW discommensurations and domains from apparent discommensurations and domains formed by interference between the CDW and the atomic lattice. In the lowest-temperature commensurate (C) phase, we find that the CDW is in the commensurate configuration as expected. We use the C phase to investigate the effects of multiple tips and find that shifts in the apparent registration of the CDW relative to the atomic lattice result. In the nearly commensurate (NC) phase, the CDW is in a true domain structure as evidenced by satellite spots in the Fourier transforms of the STM images. In the triclinic (T) phase, the STM data indicate that the CDW is in a striped domain phase, which is significantly different from the domain model previously proposed. Finally, in the high-temperature incommensurate (I) phase, we find unexpected satellite spots in the STM Fourier transforms, suggesting that a CDW modulation is also present in this phase.

I. INTRODUCTION

When a single system contains two periodic lattices with nonproportional periods, in the simplest case the system will be in an incommensurate state. However, in systems where there is some interaction between the two periodic properties, one term in the total free energy is often lower if the two lattices become commensurate. In this case, there is a competition between the terms in the free energy that determine the individual periodicities of the two lattices and the term that promotes their commensurability. For the appropriate magnitudes of these terms, it is possible for such a system to exist in a discommensurate state.[1] In this case, the two periodicities become locally commensurate within domains and undergo phase slips at the domain walls, called discommensurations, that preserve the average incommensurate periodicities.

Discommensurations have been found to exist in such diverse systems as ferroelectrics,[2] adsorbate monolayers on semiconductor surfaces,[3] mass-density waves in intercalated graphite compounds,[4] and charge-density waves in dichalcogenide compounds.[5] In each case, one lattice, for example the charge-density wave (CDW), adjusts its local phase so that it is locally commensurate with the other lattice, in this case the atomic lattice, within small domains. At the domain boundaries, it undergoes phase slips to maintain its correct long-range average periodicity. In several materials, especially $2H$-$TaSe_2$, these CDW discommensurations are readily observable with scanning transmission microscopy because the domains are relatively large ($\sim$300 Å).[5] However, a similar material, $1T$-TaS_2, has produced a long-standing controversy because of its much smaller expected domains ($\sim$70 Å). Various experiments that have looked for evidence of CDW discommensurations in this material have reached conflicting conclusions.[6–21] We have performed a scanning tunneling microscopy (STM) study on $1T$-TaS_2 that definitively proves the existence of discommensurations in two of its incommensurate CDW phases and suggests that they might be present in the third.

Tantalum disulfide is a layered material which forms a number of different polytypes defined by the stacking sequence of the layers. In the $1T$ polytype, the hexagonal unit cell contains a single three-layer sandwich consisting of a middle layer of Ta atoms octahedrally coordinated to the two outer layers of S atoms. The atoms within a single sandwich are covalently bonded, while the bonds between sandwiches are van der Waals bonds, allowing the crystals to cleave easily along these planes.

At all temperatures at which $1T$-TaS_2 is stable ($T < 543$ K), it exhibits a triple charge-density wave, with three standing waves oriented at 120° to each other (except in the triclinic phase where the hexagonal symmetry of the CDW is broken). From 543 to 353 K this material is in the incommensurate (I) phase. In this case the CDW is aligned with the lattice and has a wavelength of $3.53a_0$, where a_0 is the lattice constant of 3.346 Å.[6] When the material is cooled below 353 K it enters the nearly commensurate (NC) phase. In this phase the CDW is rotated away from the lattice by an angle Φ. This angle varies with the temperature, changing from about 11° at 350 K

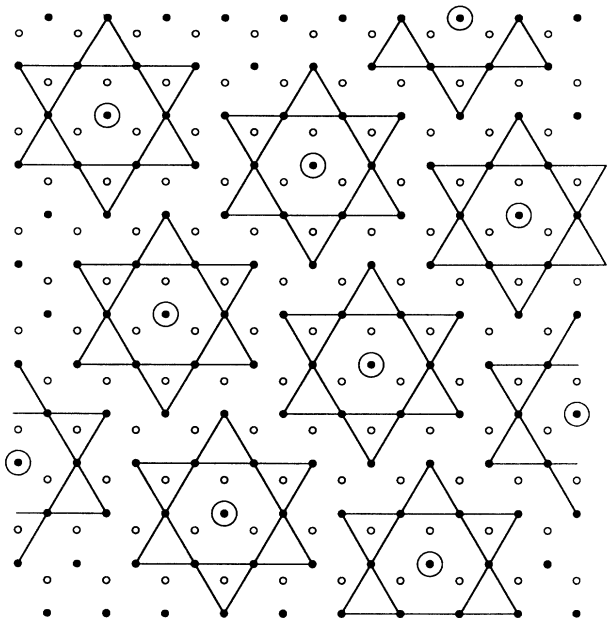

FIG. 1. Schematic of the registration of the CDW with the tantalum lattice in the commensurate (C) phase. Small solid circles represent the Ta atomic lattice, small open circles represent the S atoms on the surface, and larger open circles represent the CDW maxima formed by constructive interference of the three CDW's oriented at 120° relative to each other.

to about 13° at 250 K.[6,7] In this phase the CDW wavelength may vary slightly with temperature, but remains incommensurate. When the material is cooled below 183 K, the CDW undergoes another transition entering the commensurate (C) phase. In this case the CDW is at an angle of 13.9° and has a wavelength of $3.606a_0$, which makes it fully commensurate with the underlying tantalum lattice. Figure 1 is a schematic of the registration of the CDW on the atomic lattice in the commensurate phase. When the material is warmed from the commensurate state, it undergoes a transition at 223 K and enters the triclinic (T) phase. In this configuration, the CDW loses its hexagonal symmetry. Finally, when the temperature is raised above 283 K, the CDW again returns to the NC phase. The characteristics of each of the phases of $1T$-TaS_2 are described in Table I, and, for comparison, examples of high-resolution STM images taken in each of the four phases are shown in Fig. 2.

Theoretical calculations based on x-ray diffraction data of $1T$-TaS_2 for both the NC and T phases have predicted models in which the CDW is arranged in domains separated by discommensurations (see Fig. 3). For the NC phase,[8] the model predicts hexagonal domains with a period of about 70 Å at room temperature. The size of these predicted domains is a function of temperature because the average CDW wave vector varies with temperature. For the T phase,[9,10] a somewhat less detailed "stretched-honeycomb" model was calculated. In this case, the predicted domains are about 250 Å long and only about 40 Å wide at 225 K, and again vary in size with temperature. Both models predict that the CDW will exhibit amplitude as well as phase modulations, with the CDW amplitude greater in the center of the domains where it is commensurate and lower at the discommensurations where the CDW undergoes a phase slip of one atomic lattice unit (a_0). Although both of these models include adjustable parameters, it should be noted that the main attributes of the models are fixed, and the NC model in particular makes explicit predictions for the modulation of the CDW amplitude and phase. However, these models do not require a CDW that locks in to the commensurate wave vector inside the domains. The models can encompass cases ranging from very slight variations from a uniform orientation to a fully locked-in orientation where the CDW becomes fully commensurate within the domains.

Many experiments looking for evidence of these domains and discommensurations have been performed. Before the invention of STM, x-ray diffraction studies[9,11] not only supported the domain models, but also provided the original data upon which these models were based.

TABLE I. The phases of the CDW in $1T$-TaS_2.

Phase	Temperature (K)	Φ (deg)	Comments
Normal	$T > 543$		No CDW is known to exist. Difficult to study because crystal transforms to $2H$ polytype.
I	$543 > T > 353$	0	CDW is incommensurate and is aligned with atomic lattice.
NC	$283 < T < 353$ (warming) $353 > T > 183$ (cooling)	11–13	CDW is incommensurate and rotated away from atomic lattice. We find a hexagonal domain structure.
C	$T < 223$ (warming) $T < 183$ (cooling)	13.9	CDW is uniformly commensurate.
T	$223 < T < 283$ (warming)	12–13	CDW loses hexagonal symmetry. We find a discommensurate striped domain structure.

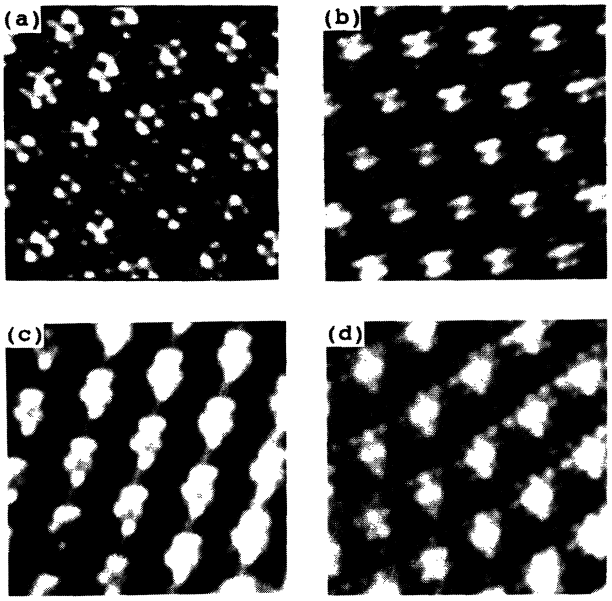

FIG. 2. Examples of high-resolution STM images, approximately 50 Å square, taken in the constant-height mode for each phase of $1T$-TaS_2. (a) I phase at 360 K; note that the CDW is aligned with the atomic lattice. (b) NC phase at 295 K; the CDW is rotated away from the atomic lattice but is not yet commensurate. (c) C phase at 143 K; the CDW is fully commensurate. (d) T phase at 236 K; similar to the NC phase.

The x-ray photoemission study of Hughes and Pollack[12] was for many years the only other piece of experimental evidence supporting the domain models. Their study showed that the x-ray photoemission spectrum of the $4f$ lines of the Ta atoms are split in the NC phase (as they are in the C phase), indicating at least two distinct inequivalent sites for the Ta atoms, rather than a continuum of sites that one would expect for a uniformly incommensurate CDW. However, three high-resolution electron microscopy studies[7,13] that achieved atomic resolution on the NC phase of $1T$-TaS_2 reported that the CDW was locally incommensurate in contradiction with the discommensuration theories. However, one of these studies,[7] reported evidence of discommensurations in the T phase.

In 1988 the first STM study that considered the question of the existence of domains in $1T$-TaS_2 was published.[14] This study found clear evidence for domains in the T phase but not in the NC phase. In a subsequent study, Gammie *et al.*[15] reported observing point discommensurations in the NC phase, in contrast with both the domain theory of Nakanishi and co-workers[8] and the previous idea of a uniformly incommensurate CDW. Later, Wu and Lieber[16] observed domainlike structure in real-space STM images of the NC phase with amplitude and phase modulation in apparent agreement with the theoretical predictions. More recent STM and atomic force microscopy measurements by Giambattista *et al.*,[17] Slough *et al.*,[18] and Garnaes *et al.*[19] showed evidence for an amplitude-modulated domain structure in the NC phase, but suggested that the CDW in this phase is continuously incommensurate across most of the sample and thus does not exhibit sharp discommensurations. However, all of these studies analyzed real-space STM images, which are inadequate to distinguish true CDW modulations from interference between the CDW and the atomic lattice.[20] Finally, Coleman, McNairy, and Slough[21] argued that the relative phases of the CDW maxima and the atomic lattice in the center of the apparent domain structure demonstrate that the observed domains are true domains and not interference effects.

We have performed extensive STM studies of $1T$-TaS_2 in all four of its phases. We use computer-generated simulations of STM images both with and without a su-

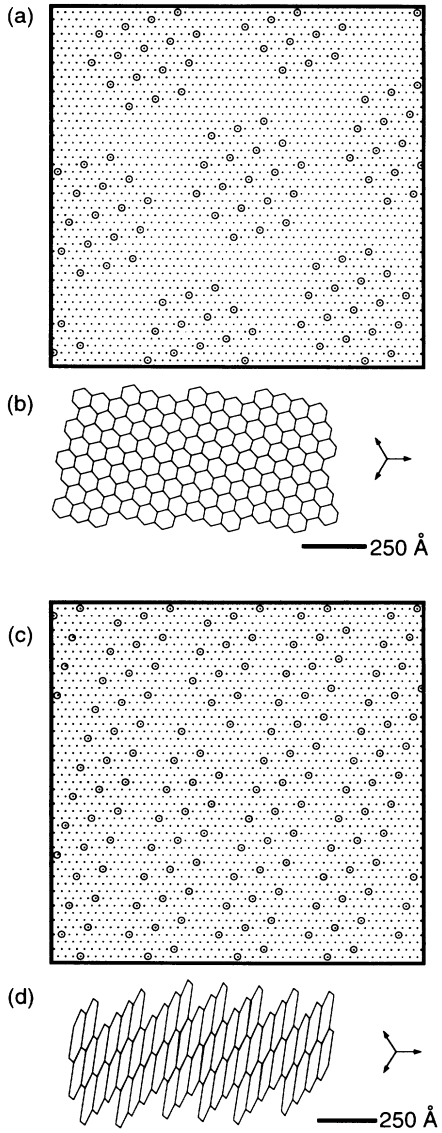

FIG. 3. Schematics of models proposed by Nakanishi and co-workers (Refs. 8,10). (a) Small-scale structure of NC phase model showing registration of CDW maxima (open circles) relative to the Ta lattice (small dots). (b) Large-scale structure of NC phase model illustrating the size and orientation of domains; solid lines are domain walls. Crystal lattice vectors are indicated at right. (c) Small-scale structure of stretched-honeycomb T phase model showing registration of CDW maxima relative to the Ta lattice. (d) Large-scale structure of T phase model illustrating size and orientation of domains.

perimposed domain structure to elucidate the most important features for distinguishing between the two cases. We show that an examination of the fine satellite structure in the Fourier transform is an unambiguous method for conclusively proving the presence of true phase and amplitude modulations in the *NC* and *T* phases; these may also exist in the *I* phase of $1T$-TaS_2. Some of our results have been previously published.[14,20,22]

II. COMPUTER SIMULATIONS

We have generated computer simulations of STM images of the *NC* phase with and without the presence of domains and discommensurations. First we consider the case where there are no amplitude or phase modulations present in the simulated CDW. Figure 4(a) shows such an image. This image was generated by superimposing three sine waves that represent the atomic lattice and three additional sine waves that produce the uniformly incommensurate CDW. The atomic lattice constant ($a_0 = 3.346$ Å) and the CDW wavelength ($\lambda_{CDW} = 11.74$ Å) have been chosen to agree with those in the *NC* phase at room temperature measured by x-ray diffraction.[6] We constructed the CDW to be at an angle relative to the lattice of $\Phi = 11.8°$, which is the average value of Φ at room temperature measured by x-ray diffraction,[6] and chose the amplitude of the CDW sine waves to be three times the amplitude of the atomic lattice sine waves, in agreement with the amplitude ratio suggested by real STM images.[23]

The method of construction of this image becomes more clear upon examination of the Fourier transform, shown in Fig. 4(b). This figure clearly shows that the only Fourier components in the image are at the fundamental frequencies of the CDW and the lattice. Nevertheless, by modifying the gray scale in the real-space image, we resolved apparent "domains," caused by the beating of these two sets of frequencies. Figure 4(c) is identical to Fig. 4(a) except that the cutoff level for the gray scale on the computer screen was adjusted to emphasize only the brightest points in the image. This procedure of modifying the computer gray scale to emphasize certain important properties of STM images has been routinely applied by many authors, and has resulted in most of the published STM images used for investigating domains in $1T$-TaS_2.

A close inspection of Fig. 4(c) will reveal that the CDW not only appears to exhibit amplitude domains, but the moiré pattern also produces apparent phase slips between the false domains. Apparent domains and phase slips are present even though the image represents a uniformly incommensurate CDW with no inherent domain structure whatsoever. These false "domains" and apparent phase slips are solely due to the interference (or beating) between the CDW and the underlying lattice which produces the observed moiré pattern.

Indeed, all of the characteristics of CDW amplitude and phase modulations that have been described in previous STM studies can be observed in the moiré pattern in Fig. 4. The apparent amplitude modulations can be observed by adjusting the computer gray scale. The ap-

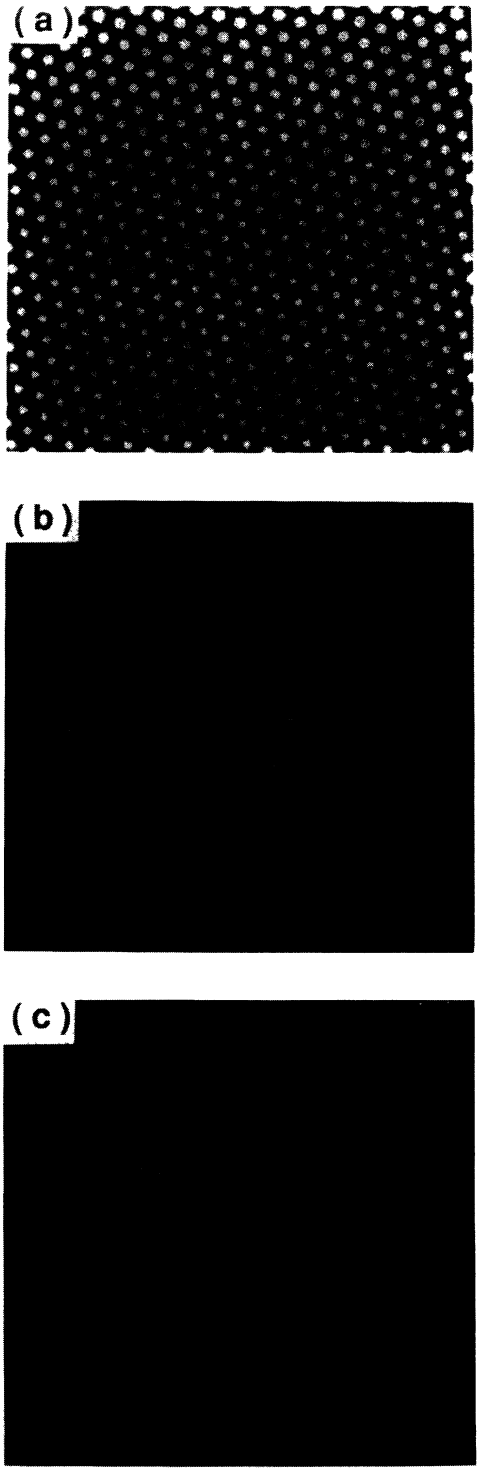

FIG. 4. Computer-generated simulation of STM images for the case where there are no domains or discommensurations in the *NC* phase. (a) Real-space image. (b) Fourier transform of (a). The six spots near the center of the transform correspond to the CDW in the real-space image, whereas the six fainter spots further from the center correspond to the atomic lattice in the real-space image. (c) Identical to (a) except that the computer gray scale has been modified to emphasize false "domains." White lines have been drawn through CDW maxima in adjacent domains to illustrate the phase shift of one lattice constant.

parent phase modulation can be seen by sighting along a line of CDW maxima at a glancing angle. The maxima in adjacent false domains do not appear to be collinear; the interference of the two lattices creates an apparent phase shift of one lattice constant between each "domain" and an adjacent one. This effect is emphasized by the lines drawn on Fig. 4(c) in two adjacent false domains. The size and orientation of the domains in the moiré pattern both agree with the values predicted by Nakanishi and co-workers discommensuration model. This is in no way unexpected. These values are dictated by the values of the average CDW wave vectors known from x-ray diffraction studies and used in the calculation of the discommensuration model. The moiré pattern even causes the CDW to appear at the commensurate angle (13.9°) inside a single "domain" [this is determined by measuring the angle relative to the lattice of the lines in Fig. 4(c)].

It is illuminating to contrast Fig. 4 with Fig. 5. Figure 5(a) is a computer simulation generated in the same way as Fig. 4 except that now the amplitude and phase modulations predicted by Nakanishi and co-workers have been added to the image. These are most easily seen in Fig. 5(b), which is a Fourier transform of the real-space image shown in Fig. 5(a). In this case, a set of reasonably intense satellite spots ring each of the fundamental CDW peaks.[24] Such satellites are always present when the CDW exhibits true domains and discommensurations. These satellites vary in intensity, and not all six possible first-order satellites are present. Those present in Fig. 5(b) were chosen to agree with those predicted from the honeycomb model of Nakanishi and co-workers in both location and intensity. For a discussion of the origin and significance of the satellite spots, see Appendix A.

Figure 5(c) is the same as Fig. 5(a) except for an adjustment of the computer gray scale. By comparing Figs. 4(c) and 5(c), one sees that unequivocal determination of the presence of amplitude domains and discommensurations in the CDW in $1T$-TaS_2 from real-space STM images is extremely difficult. However, it is equally apparent from Figs. 4(b) and 5(b) that the Fourier transform of the real-space image provides an easy method for reliable discrimination between the two cases.

Previous STM studies by other workers have relied solely on real-space STM images to attempt to identify CDW amplitude and phase modulations. Since the authors did not adequately account for the interference effect of the two lattices, the conclusions are questionable. The tests used for the determination of the presence of domains have included (1) looking for variations in the CDW amplitude (Refs. 16–19 and 21), (2) sighting along rows of CDW maxima in the real-space image to look for phase slips (Refs. 15 and 16), (3) measuring the local angle of the CDW relative to the lattice of the real-space image and comparing it to the commensurate angle of 13.9° (Refs. 14, 16, and 18), (4) examining the fine structure of the real-space images of the CDW to find areas where the CDW maxima or minima appear identical, thus proving local commensurability (Refs. 14, 16, and 17), (5) measuring the apparent domain size and orientation to see that they agree with those predicted theoreti-

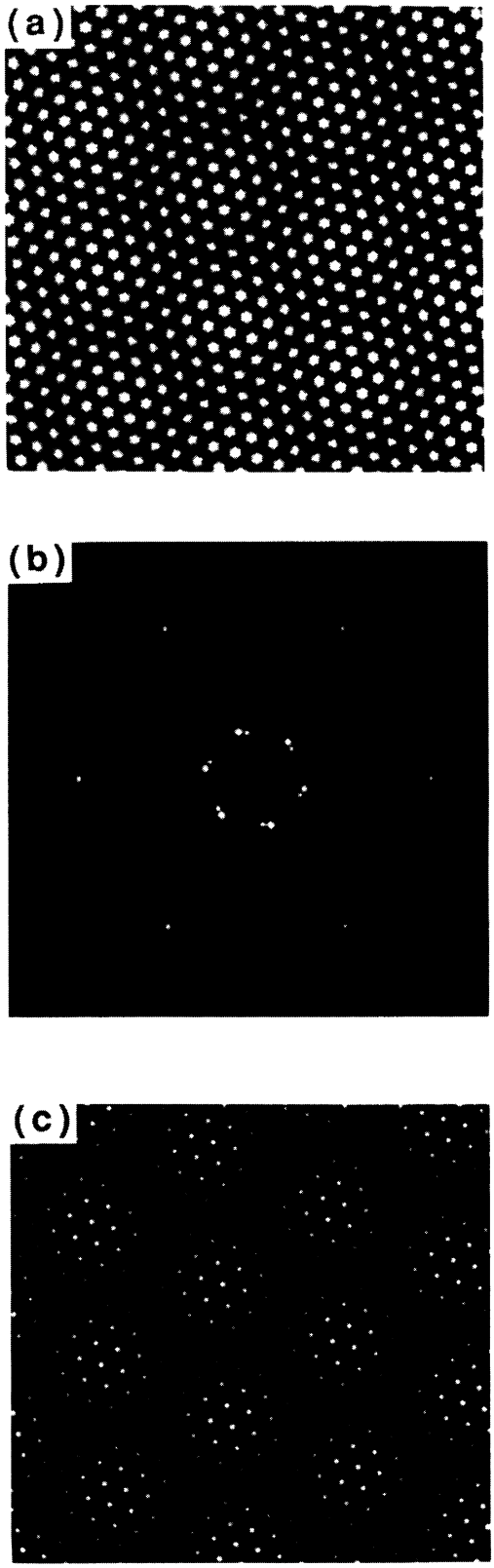

FIG. 5. Computer-generated simulation of STM images for the case where there are true domains and discommensurations in the *NC* phase. (a) Real-space image. (b) Fourier transform of (b). (c) Identical to (a) except that the computer gray scale has been modified to emphasize the domains.

cally (Ref. 16), (6) examining the Fourier transform of the real-space data for a spot at the commensurate wave vector (Ref. 19), and (7) examining the apparent phase of the CDW and the atomic lattice at the center of the apparent domains to distinguish between true domains and interference artifacts (Ref. 21).

Of these tests, (1), (2), and (3) fail because, as shown in Fig. 4(c), the moiré pattern passes them so they do not prove the existence of true domains. In addition, test (3) and test (4), are faulty because they check only for a fully locked-in domain structure. It is interesting to note that different authors have reached opposite conclusions about the real-space images using these second two tests.[25] Test (5) fails because the apparent domains produced by the moiré pattern must have the same size and orientation as true domains would, so this test cannot be used to differentiate between them. Test (6) fails because a spot at the commensurate wave vector is not expected even in the domain model. Test (7) generally fails because the apparent phase of the CDW and the atomic lattice can be altered in an indeterminate way in a STM image that is produced by simultaneously tunneling to several atoms on the tip, a common occurrence, as will be explained at greater length in the section of this paper on the *C* phase. Thus, it is clear that determining the presence or absence of domains in $1T$-TaS_2 from real-space images alone is extremely difficult.

III. STM EXPERIMENTS

A. Experimental procedure

We have described our STM elsewhere.[14] This microscope operates at atmospheric pressure, either in air or immersed in a liquid. We cleave the samples while they are immersed in a bath of hexadecane to keep the sample surface from being exposed to air. For the images taken at room temperature, we acquire the STM pictures with a thin film of hexadecane on the surface of the sample. This layer of oil appears not to affect the STM images[14,26] and usually results in higher-quality images than if the sample is exposed to air. For images taken at lower temperatures, the can in which the STM is enclosed is filled with *n*-pentane, which readily dissolves the hexadecane off the sample surface. The sample, continuously immersed in pentane, can then be cooled to the freezing point of pentane, 143 K, without ever having been exposed to the atmosphere.

We control the temperature of the microscope by immersing the can containing the STM in a Dewar which contains a thermal bath. Although the most stable STM images are acquired using a bath at its melting point to minimize thermal drift, it was possible to take STM pictures with a thermal drift rate of up to 3 K/h. The images at 143 K were taken with a bath at the melting point of *n*-pentane, those at 215 K were taken with a bath at the melting point of *n*-octane, and those at 273 K with a bath at the melting point of ice. We took the images at room temperature with no thermal bath, and those above room temperature with a bath of electrically heated mechanical vacuum pump oil. For the images taken below room temperature, the can containing the STM was filled with *n*-pentane, both to dissolve the hexadecane and to provide better thermal contact with the bath, while above room temperature, the can was filled with hexadecane to improve the thermal stability of the STM.

All of the images in this report were taken in the "constant-height" mode, where the tunneling current is used as the intensity of the image. We used this mode because we found it produced cleaner images on $1T$-TaS_2. Each image of 256×256 pixels was recorded in about 1.5 sec. The images were taken under a range of tunneling conditions, with the bias voltage on the sample between 1 and 100 mV and the tunneling current ranging from 2 to 5 nA. Although a lower tunneling resistance usually produced superior images, the images were not very sensitive to the exact tunneling parameters, including the polarity of the bias voltage.

One experimental aspect of the search for satellite spots in the Fourier transforms of our real-space STM data needs to be mentioned before we go on to a discussion of our data: if we perform a Fourier transform (FT) of the raw data, for example, those in Fig. 6(a), it is clear that any satellite spots that might be present are difficult to detect because of the bright streaks caused by the edges of the image [Fig. 6(b)]. To eliminate these streaks and obtain the cleanest possible FT, it is necessary to apodize the STM image to minimize the effects of the image edges in the FT. To do this, we multiply the real-space data by a cosine window function

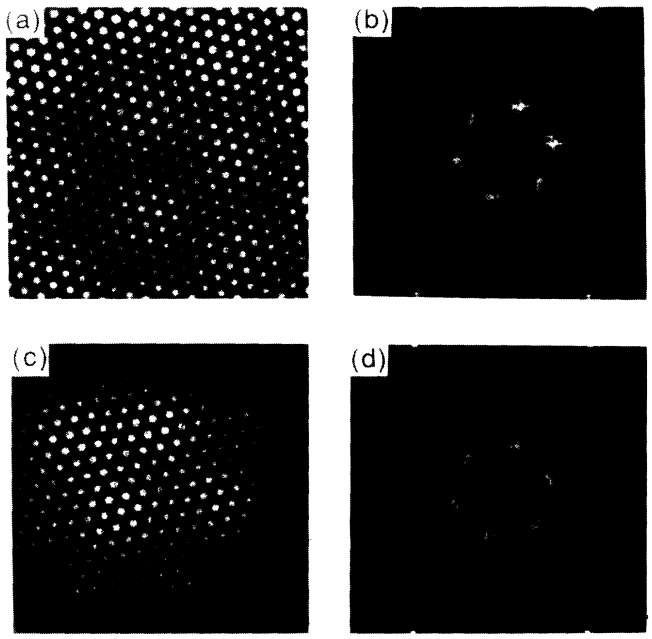

FIG. 6. (a) Computer-generated image (unapodized) of $1T$-TaS_2 in the *NC* phase [same as Fig. 5(a)]. (b) Fourier transform of (a) showing bright streaks due to image edges. (c) Same image shown in (a) after application of the apodization filter. (d) Fourier transform of (c). Satellite spots are now more clearly visible.

$$f=\{\cos[\pi(x-128)/256]-1\}\times\{\cos[\pi(y-128)/256]-1\}\ , \quad (1)$$

where x and y are the pixel indices in the data array of 256×256 pixels. Figure 6(c) shows the result of this window on the real-space image while Fig. 6(d) is a FT of the apodized image. In this figure the satellite spots around both the first-order and higher-order CDW spots are clearly visible. For this reason, the STM data presented in this report were apodized before being Fourier transformed.

The $1T$-TaS_2 single-crystal samples used in this study were synthesized using standard iodine vapor transport techniques.[27]

B. Commensurate phase

To understand the more complicated and interesting *NC*, *T*, and *I* phases, it is necessary first to understand the commensurate structure seen in the commensurate (*C*) phase at temperatures below 180 K. It is well known from x-ray studies[6] that in the *C* phase the CDW forms a hexagonal superlattice with a $\sqrt{13}\times\sqrt{13}$ unit cell rotated 13.9° from the atomic lattice. The CDW maxima are centered on 13-Ta-atom clusters arranged on a star-of-David pattern as was shown in Fig. 1. Figure 7 shows several filtered STM images of $1T$-TaS_2 taken in the *C* phase at 143 K. In these images, both the CDW and the underlying atomic lattice are visible. Moreover, it is evident that the CDW is commensurate with the atomic lattice in these images because the fine structure of each CDW maximum in an image is identical to all the other maxima in that image.

In the *C* phase as well as the other CDW phases we find that the CDW supercell can be rotated counterclockwise (α rotated in the notation of Wilson, DiSalvo, and Mohajan[28]), as in Fig. 7(a), or clockwise (β rotated), relative to the lattice, as in Fig. 7(b). X-ray diffraction experiments show that these two related superstructures can coexist in the same sample.[6] On one occasion we found adjacent areas of α and β rotation, but were unable to image the boundary region. In all other cases, we have observed only one type of rotation across the entire surface area accessible to our microscope (about 1 μm^2 at room temperature).

One surprising property observable in Fig. 7 is the asymmetry of the CDW maxima. If the CDW in the tantalum layer forms the star-of-David pattern shown in Fig. 1, as has been the assumption in the field for many years, then the registration of the CDW in the sulfur layer should have an $a_0/\sqrt{3}$ displacement from the tantalum layer as illustrated in Fig. 8(a). This image is a computer-generated model of a STM image of $1T$-TaS_2 in the *C* phase, similar to those shown in Figs. 4 and 5 for the *NC* phase. However, in this case the parameters of the image have been chosen to produce a commensurate CDW with a $\sqrt{13}\times\sqrt{13}$ superstructure. The offset of the atoms relative to the CDW maxima in this image has been chosen to agree with the $a_0/\sqrt{3}$ offset expected between the surface sulfur atoms and the CDW maxima centered on tantalum atoms one layer down. Comparison of Fig. 7 and Fig. 8(a) reveals that the asymmetry in the real STM images of $1T$-TaS_2 in the *C* phase cannot be explained by the phase shift introduced by the $a_0/\sqrt{3}$ displacement between the surface sulfur atoms and the underlying tantalum atoms which support the CDW. It is also clear that such asymmetric maxima cannot be explained by assuming that the STM images the tantalum one layer below the sulfur atoms, in which case the CDW maxima would appear to have an atom in the center with the greatest intensity ringed by six atoms of lesser intensity. In addition to the problem of the asymmetric maxima, we also find a wide variety of apparent atomic registrations in our *C* phase STM images (see Fig. 7).

The explanation for these observations comes from a well-known property of STM images: the STM can produce multiple images that have been superimposed.[29] This occurs when the STM tip terminates in multiple atoms through which the tunneling current passes. Since these two or more atoms can be at an arbitrary distance from and orientation to each other, as well as at different heights above the surface, the effect is to add together

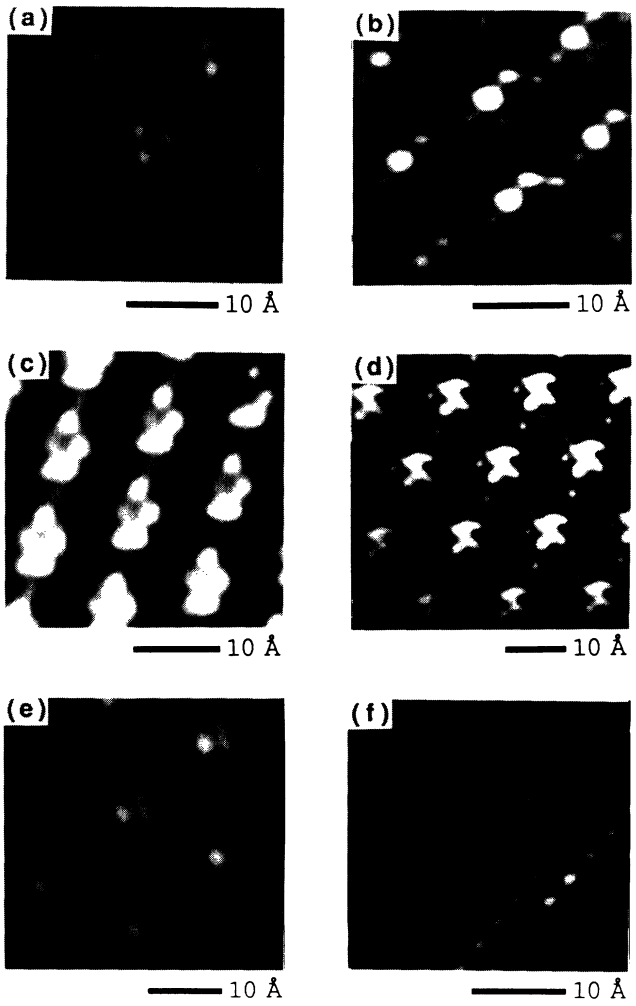

FIG. 7. Six examples of the variety of registrations we observe in STM images of the *C* phase. All images have been peak filtered (Ref. 14). (a) and (c) are in the α phase while (b), (d), (e), and (f) are in the β phase.

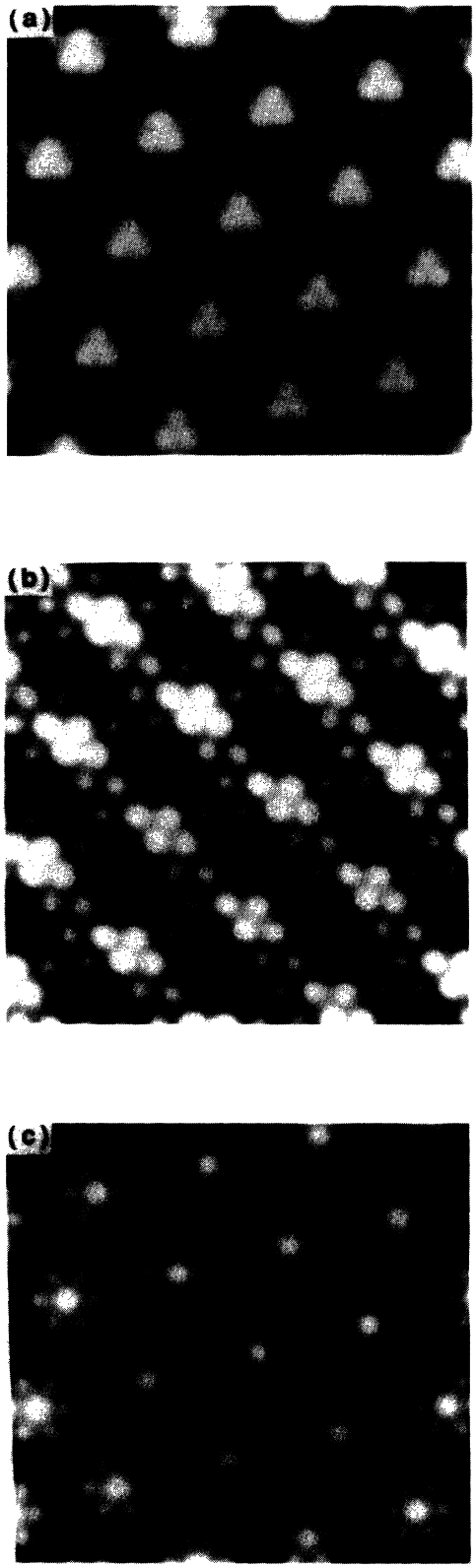

FIG. 8. Computer simulations of ideal data for the C phase. (a) Simulation of ideal STM data showing S atoms and the commensurate CDW. (b) Simulation of double-tip data; two images of (a) were offset from each other and added together to generate this image. (c) Simulation of triple-tip data, made by superposing three copies of (a) offset by lattice constants.

multiple STM images with an arbitrary offset and relative amplitude. This effect is present in many STM images of materials such as graphite.[29,30]

In order to elucidate the types of effects such multiple tips can have on a STM image, we display computer simulations of multiple-tip data in Figs. 8(b) and 8(c). We generated these images by multiplying Fig. 8(a) by an attenuation factor and adding a lateral offset and then adding the result to the original Fig. 8(a). This procedure produces images with asymmetrical CDW maxima similar to those seen in the real STM data shown in Fig. 7. Similar simulations can produce images that mimic any other atomic registration by simply varying the offset and relative amplitude of at least two separate images which are then added together.[31]

We have further verified the fact that multiple tunneling tips produced many of our STM images by a careful examination of the relative phases of the three CDW fundamental peaks in the FT's of our images. The superposition of images offset by an arbitrary amount does not introduce new Fourier components into the resultant image, but rather alters the relative phases of the peaks. By measuring the phase of each of the peaks and adding these numbers together, we produced a relative phase for the CDW's in that image. The relative phase is 0° for the simulation shown in Fig. 8(a). Experimentally we found that this relative phase varied from 0° to 360°, and an analysis of 50 of our best images did not even produce a peak in the distribution of these phases. On the contrary, the measured relative phase appeared to be random. From this we conclude that the majority of our images are made with multiple tips.

However, we stress that multiple-tip effects do not alter the distribution of Fourier peaks, including the satellite peaks due to domain structures described in Sec. II. Multiple imaging tips can change the relative phase and amplitude of the satellite spots, but cannot affect their positions. Fourier analysis continues to be a valid technique for the identification of true domain structure in the presence of multiple-tip effects.

The complication of STM images by multiple tips can also explain the findings of Raina *et al.*[32] on $1T$-$TaSe_2$, a material that has a commensurate CDW at room temperature which is identical to the commensurate low-temperature CDW in $1T$-TaS_2. This study carefully documents the types of apparent CDW registrations observable on $1T$-$TaSe_2$, but attributes them to real changes in the registration of the CDW relative to the lattice. Since there is no supporting evidence from other experimental techniques that the CDW is not in the accepted star-of-David configuration, it is more probable that these apparent registration changes are due to changes in tunneling-tip geometry similar to those seen in studies of graphite.[29,30]

Multiple-tip images are also the reason to disqualify test (7) in the earlier discussion of the work to differentiate true domains from interference effects in the NC phase. This test relies solely on the registration of the atoms with the CDW maxima at the center of the apparent domains to differentiate between true domains and interference effects.[21] Since the appearance of the CDW

maxima can be altered arbitrarily by multiple-tip effects and since multiple tips are common, a test which relies on the appearance of the maxima is unsatisfactory. Indeed, a published atomic-resolution image purporting to show the domain structure in the *NC* phase does not show the expected registration at the domain centers [as shown in Fig. 8(a)], but instead shows a four-atom CDW maximum similar to that shown in Fig. 8(b) [see Fig. 3(c) in Ref. 16(a)].

In the following discussion of the *NC*, *T*, and *I* phases, we rely extensively on the measurement of satellite structure near the CDW peaks in Fourier-transformed images. To verify that these satellite peaks are not caused by an artifact of the imaging process or of the Fourier transform, we show a *C* phase image and its FT in Fig. 9. In order to make any possible satellites apparent in the Fourier transform, we have saturated the gray scale so that a pixel with one-sixteenth of the CDW peak intensity appears as white. As expected, the six intense CDW peaks in the center of the FT [Fig. 9(b)] have no nearby satellites because the *C* phase has no discommensurate domain structure. Satellite peaks occur only when a periodic domain structure is present.

C. Nearly commensurate phase

In the *NC* phase, the CDW is not commensurate, but is oriented relative to the atomic lattice at an average angle Φ that is less than the commensurate angle of 13.9°. This temperature-dependent angle and the CDW wavelength are the factors which determine the size of the domains predicted by Nakanishi and co-workers.[8] At the higher temperatures, the predicted domains are only a few CDW wavelengths across, reducing the number of CDW maxima or minima inside the domain to about seven. This can be seen in Fig. 10(a), a STM image of 1*T*-TaS_2 taken at 343 K. In this image an apparent amplitude modulation is present, but as was discussed in Sec. II, this could be due to a moiré pattern. The very small size of the apparent domains at this temperature makes the determination of true domains from the real-space data exceedingly difficult.

As was shown in Sec. II, the presence or absence of satellite spots of moderate intensity in the FT is the key to

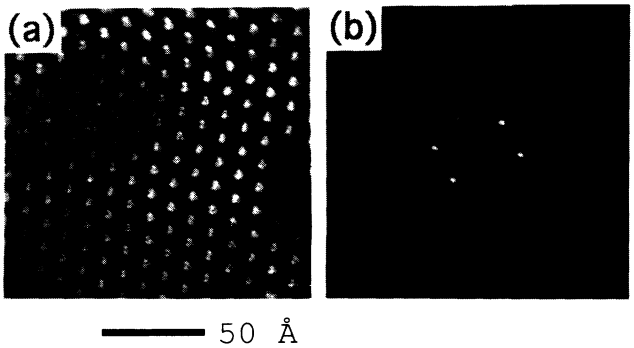

FIG. 9. (a) STM data in the *C* phase at 143 K. (b) FT of (a) with the central region enlarged by a factor of 2. Note that no satellite spots are present in the *C* phase.

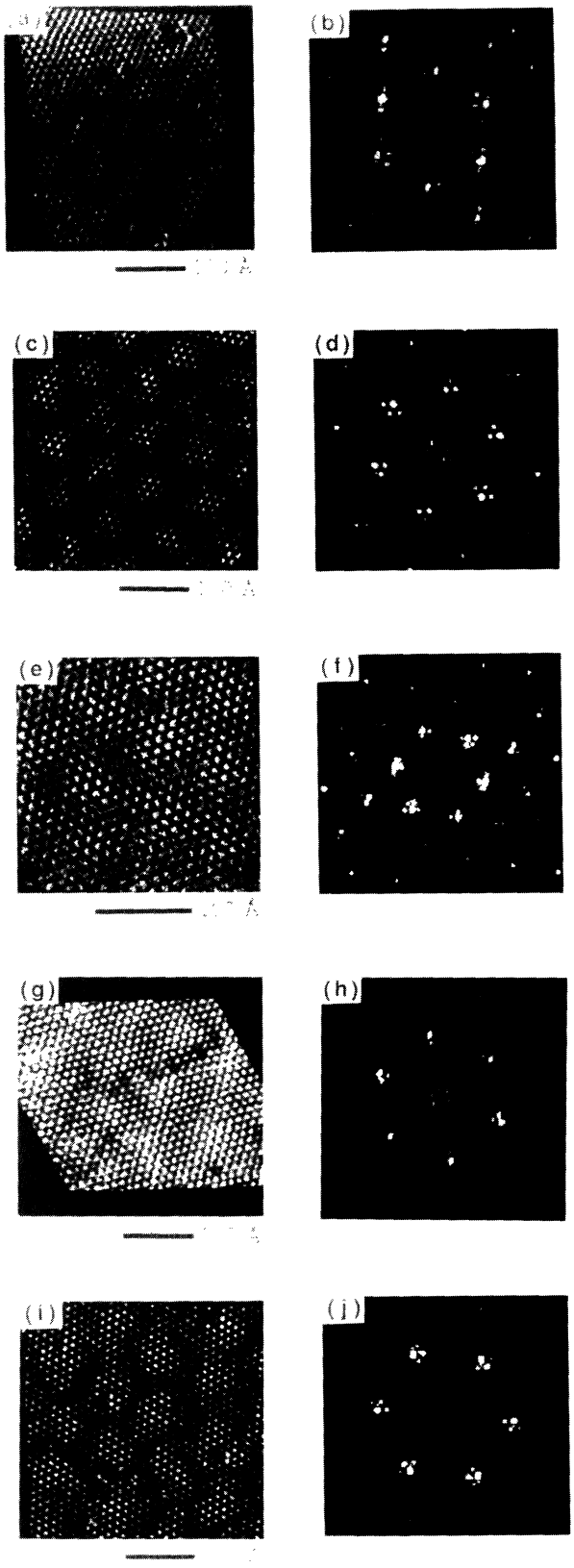

FIG. 10. (a) STM data at 343 K. (b) FT of (a). (c) STM data at 295 K. (d) FT of (c). (e) STM data at 273 K. (f) FT of (e). (g) STM data at 225 K. (h) FT of (g). (i) STM data at 215 K. (j) FT of (i). Central regions of the FT's are enlarged by a factor of 2 for better clarity of the satellite spots.

solving this problem. Figure 10(b) is the FT of 10(a). Similarly, Figs. 10(c), 10(e), 10(g), and 10(i) are the real-space STM images at 295, 273, 225, and 215 K, respectively, and Figs. 10(d), 10(f), 10(h), and 10(j) are their respective FT's. These figures clearly prove that the CDW in the *NC* phase is arranged into domains separated by diffuse discommensurations as predicted by Nakanishi and co-workers at all temperatures within the *NC* phase. Strong satellite spots are discernible in each of the Fourier transforms, unequivocally proving the existence of a discommensurate structure. The locations of the satellites, and even which of the satellites is the most intense, are consistent with those expected from the honeycomb model[8] [see Fig. 5(b)]. In addition, as shown in Fig. 11, by using the coordinates and intensities of the satellites, we have constructed graphs of the CDW amplitude, the phase relative to a commensurate CDW, and the derivative of the phase at each temperature. (See Appendix B for an explanation of this procedure.) These graphs clearly show areas where the CDW phase is nearly constant (i.e., the CDW is commensurate) and the CDW amplitude is enhanced, separated by regions of decreased CDW amplitude and rapidly changing phase (the discommensurations).[33]

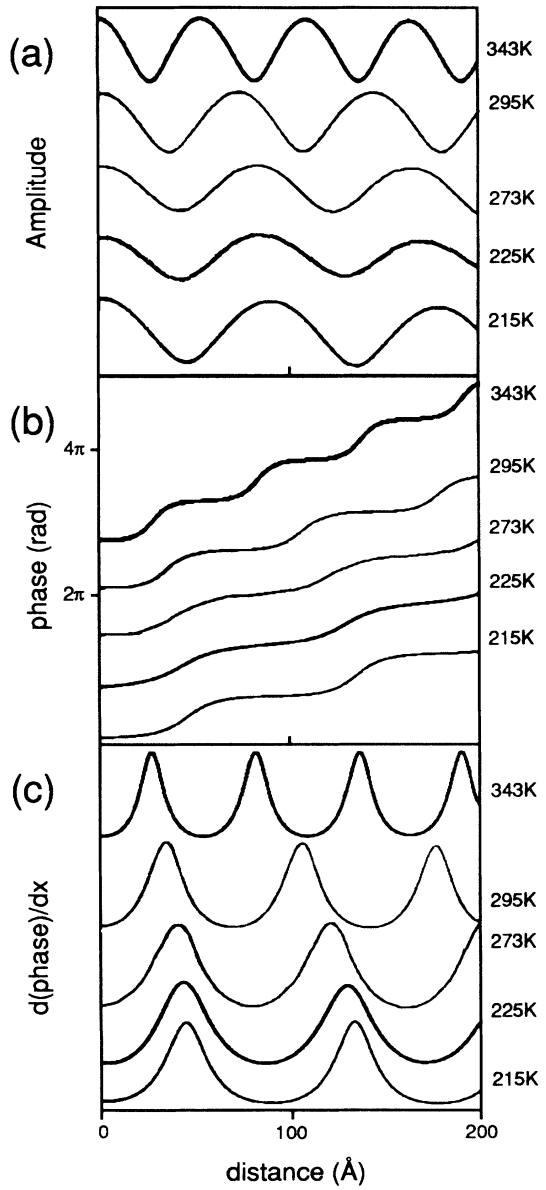

FIG. 11. Graphs generated from coordinates and intensities of the satellites in the FT's shown in Fig. 10; (a) CDW amplitude vs distance, (b) CDW phase vs distance, (c) derivative of CDW phase vs distance.

To test for a true lock-in of the CDW in the commensurate region inside domains, we have examined our FT's for second-order satellite spots. These second-order spots would have to be present for a complete lock-in to exist, because then the CDW domain modulation envelope would have to deviate from a sine wave. We found that, at the location of the potential second-order satellites, the amplitude of the FT is $<2\%$ of the amplitude of the CDW fundamental peak. This value is five times smaller than the expected amplitude of the strongest second-order satellite in the case where the CDW has locked in over the entire domain.[8] From this we conclude that the CDW phase varies over a significant portion of the domain in the *NC* phase and therefore should *not* be considered to exhibit true lock-in.

This conclusion can be verified by a close examination of Fig. 11. Although the CDW amplitude clearly varies from inside the domain to the domain wall, it never flattens out at a constant height inside the domain, as would be the case for a locked-in CDW. Likewise, as illustrated in Fig. 11(c), the CDW phase does not become constant inside the domains, although its phase does change much more slowly in the center of the domains than at the discommensurations.

Using the graphs of the derivative of the CDW phase vs distance we have extracted the domain periodicity for each temperature (averaging over at least five images at each temperature). The data at 225 K were not included in this and the following figures because we had too few high-quality images. Figure 12(a) is a graph of the domain period vs temperature for our data. Within experimental error, the domain period increases linearly with decreasing temperature.

Besides domain period, the other characteristic that completely specifies the nature of the CDW domains is domain orientation. We have attempted to measure the orientation of the CDW domains at each temperature by measuring the orientation of the satellite spots relative to the CDW fundamental spots in the FT's. Unfortunately, because of the small distances between the satellites and the CDW fundamental spots, there is a large degree of uncertainty in these measurements, which are shown in Fig. 12(b). However, as will be explained shortly, in spite of the large errors these measurements are still valuable in determining the precise nature of the CDW domain structure.

We have also measured the locations of the fundamental CDW wave vectors directly from the FT's. A comparison of our measurements (again averaged over at least five images at each temperature) of the CDW angle relative to the lattice with the measurements of Ishiguro and Sato's electron diffraction study[7] is shown in Fig.

12(c). Note in Fig. 12(c) that, if the linear trend that we observe down to 215 K continues down to the transition temperature $T=183$ K, the CDW angle Φ will not make a continuous transition to the commensurate angle of 13.9° at the transition temperature. This is in agreement with the work of Ishiguro and Sato,[7] who measured a sharp jump in Φ at 183 K when they lowered the temperature of the sample.

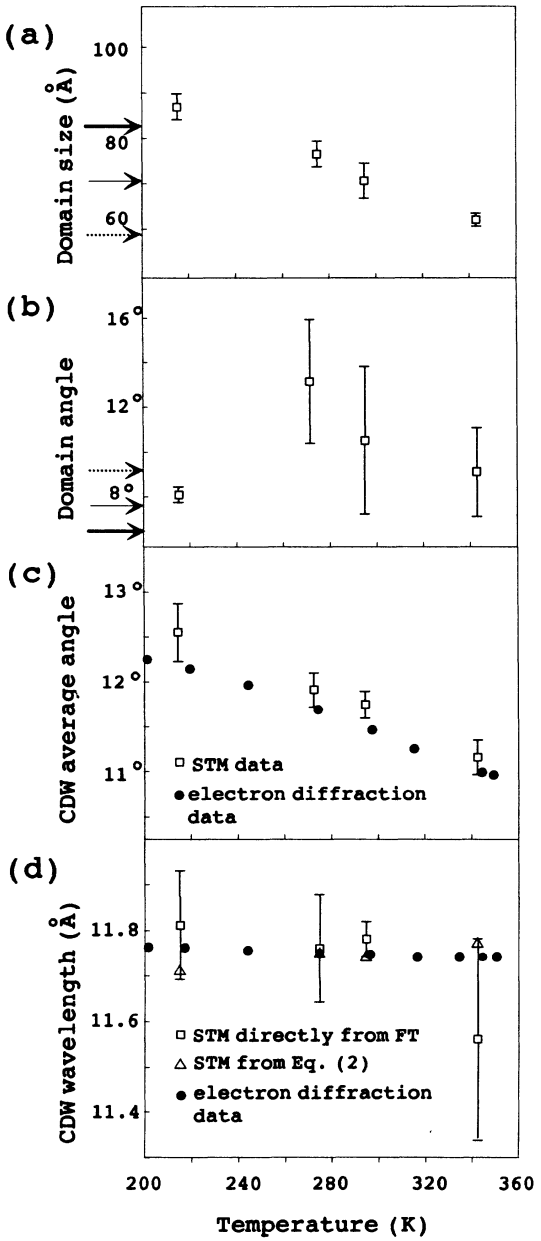

FIG. 12. Plots of CDW parameters for the *NC* phase measured from STM FT's. (a) Domain period versus temperature. (b) Domain angle versus temperature. (c) Average angle of the CDW relative to the lattice as a function of temperature (open squares) compared with previously published (Ref. 7) electron diffraction measurements (solid circles). (d) Wavelength of the CDW measured directly from the FT (open squares), and calculated from the measured CDW angle and domain periodicity (open triangles). Also plotted are results of an electron diffraction study (Ref. 7) (solid circles). The significance of the arrows in (a) and (b) is explained in the text.

Assuming that the domain periodicity occurs at the lattice and CDW beat frequency, a simple relation between the domain periodicity, the CDW angle, and the CDW wavelength is

$$\text{domain period}=a_0/\sqrt{(2\pi\delta\Phi/360)^2+(\delta\lambda/\lambda)^2}\ , \qquad (2)$$

where $\delta\Phi$ is the difference between Φ and $\Phi_{\text{commensurate}}=13.9°$ and is given in degrees, and $\delta\lambda$ is the difference between the observed λ and $\lambda_{\text{commensurate}}=12.06$ Å. This formula is derived in Appendix C. We can check the consistency of our results by comparing the CDW wavelength obtained from direct measurements of the FT and that calculated from Eq. (2). This comparison is plotted in Fig. 12(d). The wavelengths obtained by these two methods agree to within our experimental error; in addition these agree with those measured by electron diffraction.[7] Within our experimental error, the CDW wavelength does not appear to vary with temperature and has an average value of 11.73 ± 0.11 Å, which is in excellent agreement with the results of Ishiguro and Sato,[7] who found that the CDW wavelength was nearly constant in the *NC* phase with a value of about 11.75 Å.

By combining Figs. 12(a) and 12(c) we discover a subtle but interesting point about the nature of the discommensurations present in these images. To understand this point, however, it is first necessary to discuss the two possible configurations for a CDW discommensuration: the discommensuration that "compresses" the CDW wavelength and the one that "expands" the CDW wavelength.

When the CDW undergoes a discommensuration, it is required to slip one atomic lattice unit. However, the exact direction of this slip is not necessarily determined. Figure 13(a) is a schematic illustrating the two most likely choices for the direction of the slip. At the phase slip, the CDW maximum which would have coincided with the atomic position labeled 0 if it had continued in a commensurate manner, will most likely slip to either the atomic position labeled 1 or that labeled 2. If it goes to position 1, the CDW wavelength is compressed compared to the commensurate wavelength, whereas if it slips to position 2 the CDW wavelength becomes expanded. Both choices cause the CDW angle Φ, measured over several domains, to be less than the 13.9° commensurate angle, but the different angles resulting from each choice vary slightly. In their analysis of real-space STM data, Wu and Lieber concluded that the majority of the discommensurations they observed were of the compressed type.[16]

If all of the discommensurations of the CDW are of the compressed type, one possibility for the *NC* phase at room temperature is the (18×5) structure, which is technically commensurate with a repeat spacing of 18 lattice units in the *a* direction and five in the *b* direction. This is the structure that was shown in Fig. 3(a) and is redrawn in Fig. 13(b) using the open circles. The similar (19×5) structure employs expanded discommensurations and produces a slightly different CDW angle and domain periodicity. This structure is also shown in Fig. 13(b) us-

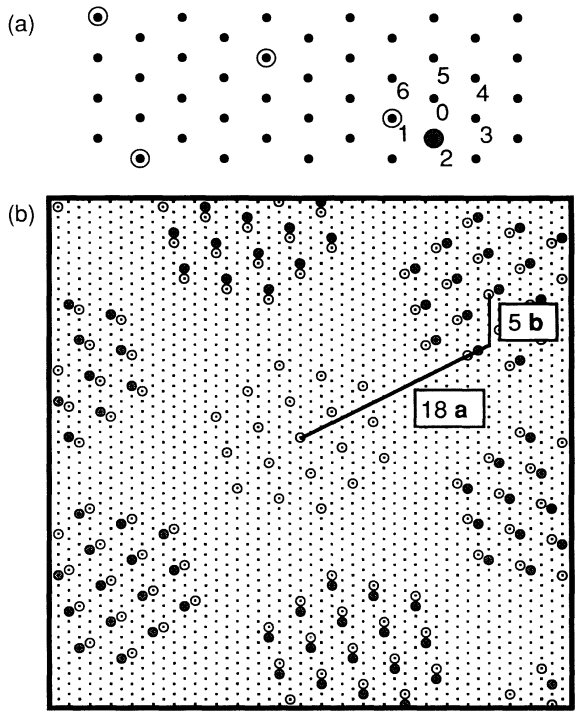

FIG. 13. (a) Schematic illustrating possible types of discommensurations. If the CDW maximum slips to the atomic position labeled 1, a discommensuration which "compresses" the CDW wavelength results. If the CDW maximum slips to the atomic position labeled 2, a discommensuration which "expands" the CDW wavelength results. (b) Schematic illustrating the (18 ×5) structure employing compressed discommensurations (open circles) and the (19×5) structure employing expanded discommensurations (gray circles).

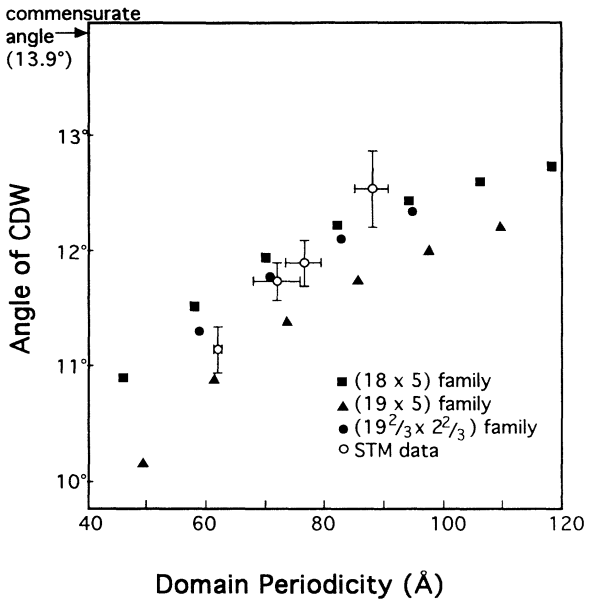

FIG. 14. Plot of the experimentally measured angle of the CDW relative to the lattice (determined by the positions of the fundamental CDW peaks in the Fourier transforms of the STM images) versus the domain periodicity (determined from the positions of the satellite spots in the Fourier transforms) compared to several possible domain families.

ing the gray circles. There exist two families of discommensurate structures, one related to the (18×5) structure using compressed discommensurations and one related to the (19×5) structure using expanded discommensurations. Within one family, the different members differ from each other only by the number of commensurate CDW wavelengths contained within each domain. The domain periodicities and CDW angles of these two families are plotted in Fig. 14, [the (18×5) compressed family plotted as solid squares and the (19×5) expanded family as solid triangles] along with our measurements of the actual CDW angle and domain period that were plotted in Figs. 12(a) and 12(c).

Examination of Fig. 14 reveals that the actual discommensurate CDW structure involves both types of discommensurations. Each point plotted in the figure is taken from our data at a different temperature. The highest-temperature point (that with the smallest domain periodicity) appears to lie closer to the family of expanded-wavelength structures, while the other points lie closer to the compressed-wavelength structures. The fact that the lowest-temperature point (that with the largest domain periodicity) lies above the line connecting the compressed-wavelength structures is not particularly disturbing. There are several other possible discommensurations, including one in which the CDW shown in Fig. 13(a) would slip to the atomic lattice position labeled 3. This choice would result in a structure with an angle much closer to the commensurate angle of 13.9° at the same domain periodicity when compared to the other two families described. A combination of different types of discommensurations between different domains would produce an intermediate structure with angle and domain periodicity values similar to those we measure.

The last question to consider in the analysis of the precise nature of the domain structure in the *NC* phase is the orientation of the domains. Wilson[34] has published an exhaustive theoretical study analyzing previous STM and electron diffraction data to determine the precise superstructure of the CDW in the *NC* phase. He concludes that the CDW at room temperature is arranged in a $(19\frac{2}{3}\times 2\frac{2}{3})$ rotated-honeycomb array which is closely related to the (18×5) array shown in Fig. 13(b). The most striking difference between these two superstructures is the orientation of the domains relative to the CDW, but the precise values of the average CDW wavelength and orientation are also different. The parameters for the two structures are given in Table II along with the values we measure for these properties from our STM images at 295 K. It is clear that, to within our experimental error, our room-temperature STM data agree with the $(19\frac{2}{3}\times 2\frac{2}{3})$ structure proposed by Wilson.[34]

However, this agreement is not maintained at the other temperatures at which we have taken data. To illustrate this point we have placed small arrows at the values of the domain size and orientation for the $(19\frac{2}{3}\times 2\frac{2}{3})$ family in Figs. 12(a) and 12(b) to compare with our experimental measurements. In both figures, the bold arrow shows the expected value for the $(22\frac{2}{3}\times 3\frac{2}{3})$ structure (presumably

TABLE II. Comparison of STM data at 295 K with domain models.

Domain structure	CDW angle Φ	CDW wavelength λ (Å)	Domain orientation relative to CDW
(18×5)	11.93°	11.68	1.96°
$(19\frac{2}{3}\times2\frac{2}{3})$	11.76°	11.72	7.62°
STM data at 295 K	11.73° ±0.16°	11.78 ±0.12	10.6° ±3.3°

present below room temperature), the middle arrow that of the $(19\frac{2}{3}\times2\frac{2}{3})$ structure (proposed by Wilson[34] to be present at room temperature), and the dashed arrow shows that of the $(16\frac{2}{3}\times1\frac{2}{3})$ structure (presumably present above room temperature). The particular discrepancies that we wish to point out are (1) the domain period at 273 K falls exactly between two of the choices of the $(19\frac{2}{3}\times2\frac{2}{3})$ family, and (2) the two lower-temperature domain orientation measurements do not agree with that of the $(22\frac{2}{3}\times3\frac{2}{3})$ structure. Even so, it should be noted that the domain orientation angles of the $(19\frac{2}{3}\times2\frac{2}{3})$ family are much closer to the observed angles than those of either the (18×5) or the (19×5) families, which would all be $<3°$. As a further check, the family of superstructures related to the $(19\frac{2}{3}\times2\frac{2}{3})$ superstructure is also plotted in Fig. 14 using the small solid circles. When these two parameters are taken together, except at room temperature, none of these structures is within the experimental error of our data points.

In addition, both our STM data and the electron diffraction data of Ishiguro and Sato[7] indicate that the CDW domain structure changes more or less continuously as the temperature is lowered. If the CDW were to adhere strictly to a specified family of superstructures, such as those related to the $(19\frac{2}{3}\times2\frac{2}{3})$, not only would the size and orientation of the domains be constrained to increase in discrete jumps as one more commensurate CDW wavelength was added to each domain, but, since the CDW average angle and wavelength are also specified for each member of the family, these quantities are also constrained to increase in discrete jumps. Based on the measurements of domain period, we would expect at most four members of the $(19\frac{2}{3}\times2\frac{2}{3})$ family to be present over the *NC* phase temperature range. However, the electron diffraction measurements, shown in Fig. 12(c), clearly show that the CDW average angle increases smoothly as the temperature is lowered. In addition, the CDW wavelength is expected to vary from 11.67 Å for the $(16\frac{2}{3}\times1\frac{2}{3})$ structure to 11.80 Å for the $(25\frac{2}{3}\times4\frac{2}{3})$ structure, while the electron diffraction measurements shown in Fig. 12(d) show that the CDW wavelength actually stays between 11.74 and 11.76 Å.

Therefore, we believe that, although the CDW domain superstructure appears more closely related to the $(19\frac{2}{3}\times2\frac{2}{3})$ family than to other structures such as the (18×5) family, our STM data do not support the conclusion that the CDW superstructure adheres to any particular family of superstructures, or that it jumps discontinuously from one to the next in a family of superstructures. On the contrary, even in the real-space STM images the CDW domains appear to be nonuniform [see Figs. 10(a), 10(c), 10(e), 10(g), and 10(i)], with some domains appearing to be of unusual sizes or off center relative to the other domains in a single image.

One final point about the CDW structure in the *NC* phase is that, contrary to Ishiguro and Sato,[7] who described the *NC* phase as having domains only on warming from the *T* phase, we find that the domains and discommensurations as evidenced by the satellite structure are present in the *NC* phase both when the sample is cooled from the *I* phase and when it is warmed above the *T* phase. We heated a single sample to 390 K for 48 h to insure that the CDW would be in the *I* phase and then allowed it to cool to room temperature. After verifying the existence of the satellite spots in the FT, we then cooled it to 77 K for 48 h and again checked for satellite spots after warming it up to room temperature. Two examples of our FT's showing clear satellite spots both upon warming and cooling are shown in Fig. 15.[35] Our measurements are not precise enough to discern the differences in the CDW wavelength and angle when data are taken at the same temperature but on different sides of the hysteretic curve of $1T$-TaS_2, as reported by Ishiguro and Sato.[7] However, we can confidently say that domains and discommensurations are present at room temperature regardless of the thermal history of the sample.

In summary, in the *NC* phase of $1T$-TaS_2 we have shown unequivocally that a true discommensurate domain structure exists, and have analyzed this structure at 215, 225, 273, 295, and 343 K. The domain size increases monotonically with decreasing temperature, but

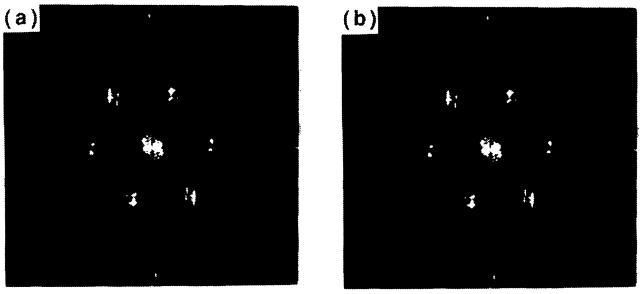

FIG. 15. (a) Fourier transform of STM data in the *NC* phase at 295 K just after the sample was cooled from the *I* phase. (b) Fourier transform of STM data of $1T$-TaS_2 in the *NC* phase at 295 K just after the sample was warmed from the *T* phase. Satellite spots are clearly visible in both FT's.

the angle of the CDW relative to the lattice does not continuously approach the commensurate angle at the transition temperature. In addition, we found it unlikely that the $(19\frac{2}{3}\times 2\frac{2}{3})$ structure, or any other rigorously commensurate superstructure, adequately describes the complicated domain superstructure observed in the STM images.

D. Triclinic phase

Unlike the nearly commensurate phase, $1T$-TaS_2 in the triclinic (T) phase (present only on warming $1T$-TaS_2 from the commensurate phase) loses its hexagonal symmetry. This means that in this phase the domains are not hexagonal, but are long and narrow. This has the effect of making the determination of their presence from real-space data somewhat less difficult because the long narrow domains provide many CDW maxima or minima to compare for a similarity of their fine structures. A STM study reporting domains in the T phase of $1T$-TaS_2 used this technique of comparing CDW maxima.[14] However, as was explained in Sec. II, the best way to determine unequivocally the presence of CDW domains and discommensurations is to examine the FT for satellite spots.

A STM image of $1T$-TaS_2 in the T phase at 225 K is shown in Fig. 16(a). This image is too large to resolve the atomic lattice; the smallest visible periodic features are the CDW maxima. Although surface defects obscure any obvious CDW domain structure, close inspection reveals long stripes running diagonally across the image from upper right to lower left. We interpret these stripes as CDW domains, where the brighter stripes are regions of enhanced CDW maxima, separated by darker lines of diminished CDW amplitude, similar to the images of the *NC* phase. From an analysis of six images from three samples we find the stripes have an average width of 68±5 Å and make an angle of 28°±5° with the CDW translation-vector direction. The stripes appear to be at least as long as the largest scan (500 Å) that we can obtain.

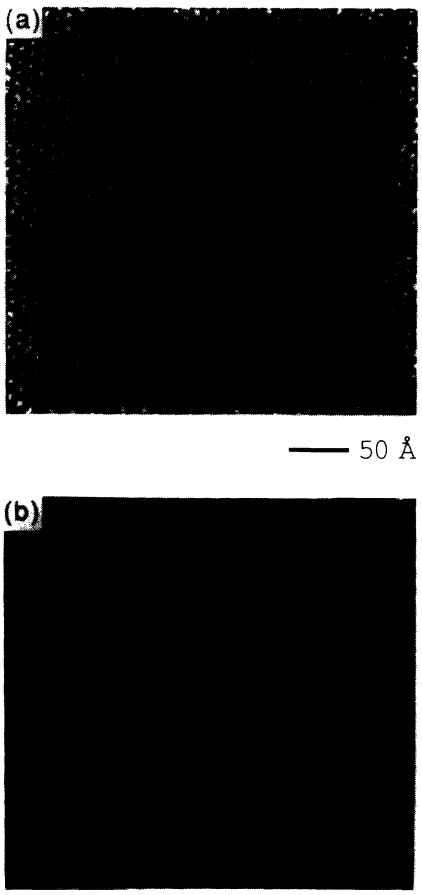

FIG. 16. (a) Real-space STM data of the T phase at 225 K. (b) Fourier transform of (a).

Figure 16(b), the Fourier transform of Fig. 16(a), confirms this identification of a stripe domain structure, showing three pairs of strong peaks which are the fundamental CDW peaks. Clear satellite peaks occur near two of the three opposing pairs of CDW peaks. This satellite structure demonstrates a true domain modulation of the T phase CDW.

Our measurements of the orientation and length of these domains are inconsistent with the stretched-honeycomb model Nakanishi and Shiba[10] proposed based on a previous x-ray diffraction study,[9] which is shown in Fig. 3(d). The stretched-honeycomb model has domains with a width of 38 Å, a length of 250 Å, and an orientation of the long dimension of the honeycomb at an angle of about 1° with respect to the CDW translation vector. In the x-ray diffraction study on which the stretched-honeycomb model is based, only the CDW fundamental peaks were measured, and the domain model was inferred from these peaks, i.e., the satellite spots in the diffraction pattern were not measured.[9] In order to resolve the discrepancies between this previously accepted model and our data we performed an x-ray diffraction study which is described elsewhere.[22] Careful measurements of the CDW fundamental spots *and the satellite spots* in the x-ray diffraction pattern allowed us to determine the domain configuration in the T phase in the bulk of the crystal. Both the stretched-honeycomb model of Nakanishi and Shiba[10] and the striped model generated from our recent x-ray diffraction measurements[22] are shown in Fig. 17. This figure was generated with the same computer simulation program used for Figs. 4, 5, and 7. This striped model has a domain width of 63±3 Å, a stripe length of at least 600 Å, and an orientation of 24.5°±3.5°. Comparison of Fig. 16(a) and Fig. 17, together with a comparison of the relevant domain dimensions which are summarized in Table III, lead us to the conclusion that the T phase of $1T$-TaS_2 displays this striped domain structure on the surface as well as in the bulk.[22]

E. Incommensurate phase

In the incommensurate (I) phase, present between 543 and 354 K, the CDW in $1T$-TaS_2 is aligned with the lattice, as was shown in Fig. 2(a). An earlier STM study[14] examined the transition between the I phase and the *NC* phase and determined that the transition between the two phases occurred at the surface at the same temperature as

in the bulk of the sample. This is a further indication that the CDW properties in $1T$-TaS_2 are identical in the bulk and on the surface.

Figure 18(a) is a STM image of $1T$-TaS_2 in the I phase. An interesting property of the CDW in the I phase becomes apparent only on examination of the Fourier transform, shown in Fig. 18(b). This FT shows a complicated pattern of peaks which are reminiscent of the satellite peaks present in the FT's when the CDW is in the discommensurate NC and T phases (Figs. 10 and 16). Interestingly, these "satellites" are in a significantly different orientation from those in the NC and T phases. In the case of the NC and T phases, the satellite peaks do not appear on the line through the fundamental CDW peak and the origin of the FT, which is where the "satellite" peaks occur in the case of the I phase. These extra peaks are suggestive of a modulation of the CDW in this phase as well. However, in the I phase, there is no evidence of such a modulation discernible in the real-space data. This is because the intensity of the "satellite" peaks in the FT of this phase is only 1% of the fundamental CDW peak, whereas, for instance, in the T and NC phases the satellite peaks are typically about 20% of the intensity of the fundamental CDW peak.

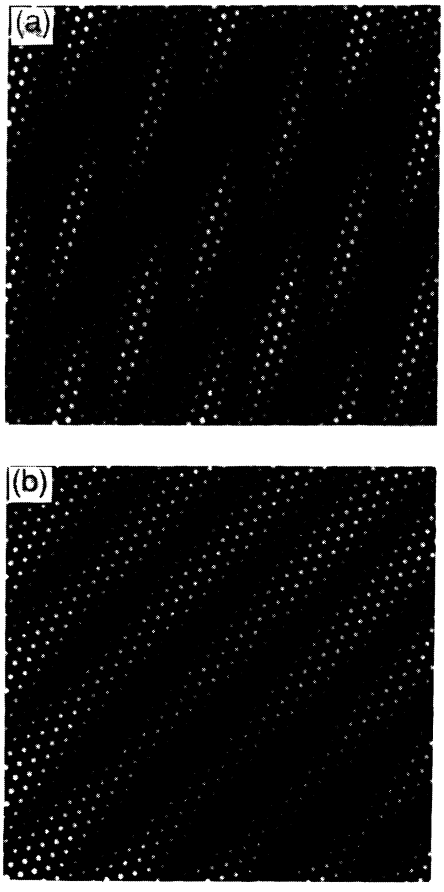

FIG. 17. (a) Computer simulation of STM data of a CDW in the stretched-honeycomb domain model of Nakanishi and Shiba (Ref. 10). (b) Computer simulation of STM data of a CDW in the striped domain model determined by Burk *et al.* (Ref. 22).

TABLE III. Comparison of T phase STM data with domain models.

Domain structure	Domain width (Å)	Domain length (Å)	Domain orientation relative to CDW
Stretched honeycomb model[a]	38±3	250±80	1°±3°
Striped model[b]	63±3	> 600	24.5°±3.5°
STM data	68±5	> 500	28°±5°

[a]Reference 10.
[b]Reference 22.

Because the observed "satellite" peaks are exactly two CDW wave vectors from the lattice peak, it is difficult to determine whether these peaks are simply second-order harmonics of a uniform CDW or if they indicate a weak but true modulation of the CDW. In order to distinguish between these choices a careful comparison of the CDW fundamental and the "satellite" peaks is required. Fourier transforms of STM data are not suitable for the precise determination of intensity ratios of the peaks. In order to resolve this question, we performed a careful x-ray diffraction study to measure the peak intensities.[36] We found that the ratio of the second-order CDW peak intensity to the first-order CDW peak intensity exceeds

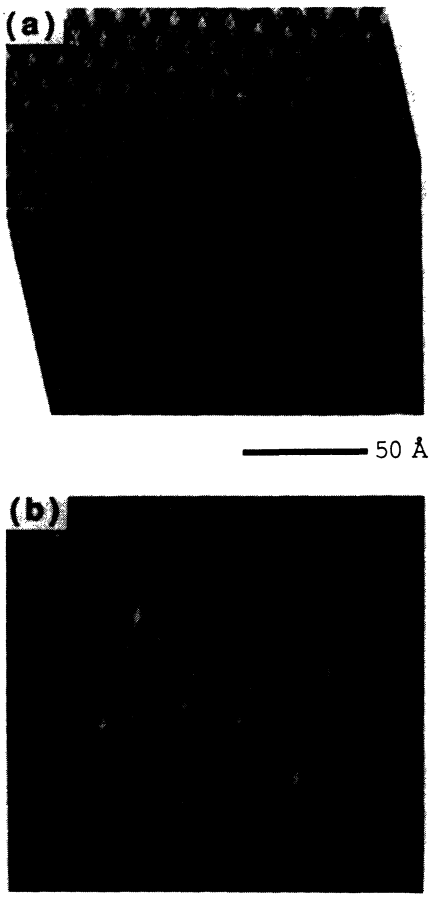

FIG. 18. (a) Real-space STM data of $1T$-TaS_2 in the I phase at 360 K. (b) Fourier transform of (a).

the value calculated for a purely sinusoidal periodic lattice distortion by a factor of 18. The excess intensity can be explained by a weak modulation of the CDW amplitude and phase with a period close to two CDW wavelengths.[36]

IV. CONCLUSIONS

We have shown that a straightforward and reliable method for determining the presence of domains and discommensurations in a CDW system is to examine the Fourier transform of the STM image for satellite spots. Using this method, we have proven the existence of CDW modulations in the *NC* and *T* phases in 1*T*-TaS_2 and have shown the possibility of a similar modulation in the *I* phase. In addition, we have shown, using *C* phase data, that multiple-tip effects can complicate the interpretation of a STM image of a CDW.

In the *NC* phase we found that the CDW exhibits a hexagonal domain configuration at all temperatures regardless of thermal history. The domain size increases monotonically with decreasing temperature, and the domain orientation relative to the CDW direction also increases slightly. The angle of the CDW relative to the atomic lattice does not continuously approach the commensurate angle at the phase transition to the *C* phase, and, to within our experimental error, we find the wavelength of the CDW to be approximately constant throughout the *NC* phase. The CDW does not lock in to the atomic lattice and it does not rigidly adhere to any particular family of rigorously commensurate superstructures.

In the *T* phase we found that the CDW is modulated by a striped domain configuration, which is significantly different from that proposed by Nakanishi and Shiba,[10] but agrees precisely with that developed by Burk *et al.*[32] from x-ray diffraction measurements of the CDW satellite positions and intensities. In the *I* phase we find that the CDW is aligned with the atomic lattice and that the FT of the real-space data displays very faint higher-order peaks suggestive of a CDW modulation.

ACKNOWLEDGMENTS

We thank F. J. DiSalvo for providing some of the samples used in this study, and X. L. Wu, P. Rauch, R. V. Coleman, and J. Garnaes for helpful discussions. This work was supported by the Director, Office of Energy Research, Office of Basic Energy Science, Materials Science Division of the U.S. Department of Energy, under Contract No. DE-AC03-76F00098 and by NSF Grant No. DMR-9017254.

APPENDIX A: ORIGIN AND SIGNIFICANCE OF SATELLITE PEAKS

The origin and significance of the satellite spots in the Fourier transforms of STM data are easy to understand. In the case of a one-dimensional discommensurate CDW, the wave function of the CDW can be written as[8]

$$\Psi_{\mathrm{CDW}}=\Psi_{\mathrm{IC}}(x)M(x)\ , \tag{A1}$$

where $\Psi_{\mathrm{IC}}(x)$ is the wave function of the uniformly incommensurate CDW and $M(x)$ is a modulation envelope. This modulation envelope can be expressed as a Fourier series in the modulation wave vector k_D,

$$M(x)=\sum f_n e^{i(nk_D x)}\ . \tag{A2}$$

Only the first two terms, $n=0,1$, in this Fourier expansion are relevant since they are much larger than the higher-order terms,[8] so that

$$\Psi_{\mathrm{CDW}}=f_0\Psi_{\mathrm{IC}}(x)+f_1\Psi_{\mathrm{IC}}(x)e^{i(k_D x)}+\cdots\ . \tag{A3}$$

Since

$$\Psi_{\mathrm{IC}}(x)=\Psi_0 e^{i(k_{\mathrm{IC}}x)}\ , \tag{A4}$$

where k_{IC} is the incommensurate wave vector, Eq. (A3) produces terms in the Fourier expansion at k_{IC} and at $k_{\mathrm{IC}}+k_D$. Generalizing to the two-dimensional case, we see that the term at k_{IC} is the fundamental incommensurate CDW peak seen in the Fourier transform and the terms at $k_{\mathrm{IC}}+k_D$ are the satellite peaks which are the signature of the modulation, i.e., of the domain structure.

APPENDIX B: CONSTRUCTION OF CDW AMPLITUDE AND PHASE FROM FT'S

The amplitude and phase domain modulation envelopes are extracted from the Fourier transforms of the real-space STM images. The envelopes shown in Fig. 11 reflect the modulation of a single CDW fundamental Fourier component induced by neighboring satellites. The procedure used to obtain and display the modulation envelope is described below.

The contribution to the real-space image of a single CDW Fourier component and its associated satellites, $\rho(\mathbf{r})$, may be expressed as

$$\rho(\mathbf{r})=\rho_0 e^{i\mathbf{k}_0\cdot\mathbf{r}}+\sum\rho_n e^{i\mathbf{k}_n\cdot\mathbf{r}}\ , \tag{B1}$$

where ρ_0 refers to the CDW fundamental Fourier component and ρ_n refers to the satellites. Here ρ_i is a complex number that represents the amplitude and phase of the Fourier component, $\mathbf{k}_i$ is the wave vector, and $\mathbf{r}$ is the real-space position. Equation (B1) may be rewritten as

$$\rho(\mathbf{r})=\rho_0 e^{i\mathbf{k}_C\cdot\mathbf{r}}\left\{e^{i(\mathbf{k}_0-\mathbf{k}_C)\cdot\mathbf{r}}\left[1+\sum(\rho_n/\rho_0)e^{i(\mathbf{k}_n-\mathbf{k}_0)\cdot\mathbf{r}}\right]i\right\}\ . \tag{B2}$$

where $\mathbf{k}_C$ is the commensurate wave vector and the term in braces is the modulation envelope $M(\mathbf{r})$. We may express $M(\mathbf{r})$ as

$$M(\mathbf{r})=A(\mathbf{r})e^{i\phi(\mathbf{r})}\ , \tag{B3}$$

where $A(\mathbf{r})$ and $\phi(\mathbf{r})$ are the amplitude and phase of the modulation envelope. Thus

$$A(\mathbf{r})=|M(\mathbf{r})| \tag{B4}$$

and

$$\phi(\mathbf{r})=\arctan\left\{\frac{\mathrm{Im}[M(\mathbf{r})]}{\mathrm{Re}[M(\mathbf{r})]}\right\}\ . \tag{B5}$$

The functions $A(\mathbf{r})$, $\phi(\mathbf{r})$, and $\phi'(\mathbf{r})$ are plotted in Fig.

11 for a specifically chosen direction of $\mathbf{r}$. The set of wave vectors $\mathbf{k}_n - \mathbf{k}_0$ are domain wave vectors. We choose the direction of $\mathbf{r}$ to make a 30° angle with respect to the domain vector which connects the CDW fundamental peak to its strongest satellite. The sense of the 30° angle is such that $\mathbf{r}$ is nearly antiparallel to $\mathbf{k}_0$. With this direction chosen for $\mathbf{r}$, the envelopes plotted in Fig. 11 reflect the modulation of the CDW along a line parallel to a row of domains.

APPENDIX C: DERIVATION OF DOMAIN PERIOD FORMULA

Here we derive an expression for the beat period between the atomic lattice and the CDW in the *NC* phase. The beat wave vector is the difference between a reciprocal lattice vector and a sum of CDW wave vectors which nearly equals the reciprocal lattice vector. The beat period is the reciprocal of the magnitude of the beat wave vector.

In Fig. 19(a) we illustrate the commensurate case. Here $\mathbf{a}^*$ is a reciprocal lattice vector and $\mathbf{k}_C^1$ and $\mathbf{k}_C^3$ are commensurate CDW wave vectors. In the commensurate case three conditions are satisfied: $3\mathbf{k}_C^1 - \mathbf{k}_C^3 = \mathbf{a}^*$, $|\mathbf{k}_C^1| = |\mathbf{k}_C^3|$, and $\mathbf{k}_C^3$ is rotated 120° counterclockwise with respect to $\mathbf{k}_C^1$. In the *NC* phase the first condition is no longer satisfied although the second two are.

In the nearly commensurate case, illustrated in Fig. 19(b), $\mathbf{k}^1$ and $\mathbf{k}^3$ are *NC* CDW wave vectors, $\mathbf{k}_B$ is the beat vector, $\mathbf{s} = 3\mathbf{k}^1 - \mathbf{k}^3$, and $\delta\Phi$ is the deviation angle of $\mathbf{k}^1$ from the commensurate angle. By similarity of triangles in the commensurate and *NC* cases,

$$|\mathbf{s}| = |\mathbf{a}^*||\mathbf{k}^1|/|\mathbf{k}_C^1| \ . \tag{C1}$$

By the law of cosines

$$|\mathbf{k}_B| = \sqrt{|\mathbf{a}^*|^2 + |\mathbf{s}|^2 - 2|\mathbf{a}^*||\mathbf{s}|\cos\delta\Phi} \ . \tag{C2}$$

Defining ε as

$$(1+\varepsilon) = |\mathbf{k}^1|/|\mathbf{k}_C^1| = \lambda_C/\lambda = 1 + (\delta\lambda/\lambda) \ , \tag{C3}$$

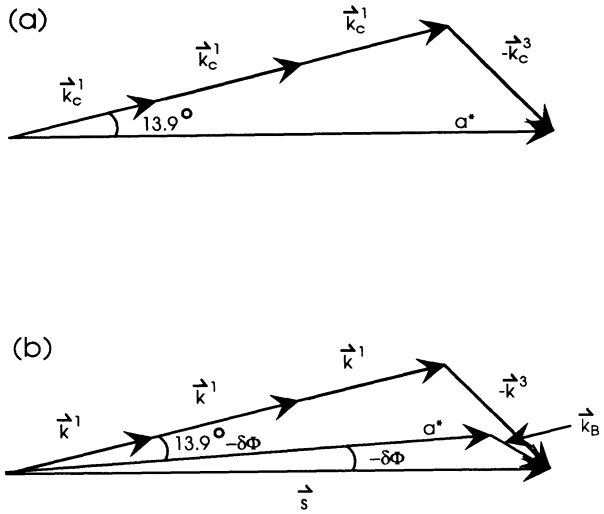

FIG. 19. (a) Schematic of the relationship between the CDW wave vectors and the reciprocal lattice vectors in the commensurate case. (b) Schematic of the relationship between the CDW wave vectors, the reciprocal lattice vectors, and the domain wave vector in the incommensurate case.

where λ_C is the commensurate CDW period and λ is the observed *NC* phase CDW period and $\delta\lambda = \lambda_C - \lambda$, we may write

$$|\mathbf{k}_B| = |\mathbf{a}^*|\sqrt{1+(1+\varepsilon)^2 - 2(1+\varepsilon)\cos\delta\Phi} \ , \tag{C4}$$

which simplifies to

$$|\mathbf{k}_B| = |\mathbf{a}^*|\sqrt{\varepsilon^2 + (1+\varepsilon)[2\sin(\delta\Phi/2)]^2} \ . \tag{C5}$$

Finally,

$$\text{beat period} = a_0/\sqrt{\varepsilon^2 + (1+\varepsilon)4\sin^2(\delta\Phi/2)} \ , \tag{C6}$$

where a_0 is the atomic lattice constant. Upon making the approximations $(1+\varepsilon) \approx 1$, since $\varepsilon \ll 1$, and $\sin\delta\Phi/2 \approx \pi\delta\Phi/360$, since $\delta\Phi/2 \approx 1°$, we obtain Eq. (2).

*Present address: Electromagnetic Technology Division, National Institute of Standards and Technology, Boulder, CO 80303.

[1]W. L. McMillian, Phys. Rev. B **14**, 1496 (1976).
[2]H. Bestgen, Solid State Commun. **58**, 197 (1986).
[3]A. B. McLean, R. M. Feenstra, A. Taleb-Ibrahimi, and R. Ludeke, Phys. Rev. B **39**, 12 925 (1989).
[4]R. Clarke, J. N. Gray, H. Homma, and M. J. Winokur, Phys. Rev. Lett. **47**, 1407 (1981).
[5]C. H. Chen, J. M. Gibson, and R. M. Fleming, Phys. Rev. Lett. **47**, 723 (1981).
[6]C. B. Scruby, P. M. Williams, and G. S. Parry, Philos. Mag. **31**, 225 (1975).
[7]T. Ishiguro and H. Sato, Phys. Rev. B **44**, 2046 (1991).
[8]K. Nakanishi, H. Takatera, Y. Yamada, and H. Shiba, J. Phys. Soc. Jpn. **43**, 1509 (1977); K. Nakanishi and H. Shiba, *ibid.* **43**, 1893 (1977).
[9]S. Tanda, T. Sambongi, T. Tani, and S. Tanaka, J. Phys. Soc. Jpn. **53**, 476 (1984); S. Tanda and T. Sambongi, Synth. Met. **11**, 85 (1985).
[10]K. Nakanishi and H. Shiba, J. Phys. Soc. Jpn. **53**, 1103 (1984).
[11]Y. Yamada and H. Takatera, Solid State Commun. **21**, 41 (1977).
[12]H. P. Hughes and R. A. Pollack, Commun. Phys. **1**, 61 (1976).
[13]M. Kuwabara, M. Tomita, H. Hashimoto, and H. Endoh, Phys. Status Solidi A **96**, 39 (1986); G. van Tendeloo, J. van Landuyt, and S. Amelinckx, *ibid.* **64**, K105 (1981).
[14]R. E. Thomson, U. Walter, E. Ganz, J. Clarke, A. Zettl, P. Rauch, and F. J. DiSalvo, Phys. Rev. B **38**, 10 734 (1988); R. E. Thomson, U. Walter, E. Ganz, P. Rauch, A. Zettl, and J. Clarke, J. Microsc. **152**, 771 (1988).
[15]G. Gammie, S. Skala, J. S. Hubacek, R. Brockenbrough, W. G. Lyons, J. R. Tucker, and J. W. Lyding, J. Microsc. **152**, 497 (1988).

[16]X. L. Wu and C. M. Lieber, (a) Science **243**, 1703 (1989); (b) Phys. Rev. Lett. **64**, 1150 (1990); (c) J. Vac. Sci. Technol. B **9**, 1044 (1991).

[17]B. Giambattista, C. G. Slough, W. W. McNairy, and R. V. Coleman, Phys. Rev. B **41**, 10 082 (1990).

[18]C. G. Slough, W. W. McNairy, R. V. Coleman, J. Garnaes, C. B. Prater, and P. K. Hansma, Phys. Rev. B **42**, 9255 (1990); C. G. Slough, W. W. McNairy, C. Wang, and R. V. Coleman, J. Vac. Sci. Technol. B **9**, 1036 (1991).

[19]J. Garnaes, S. A. C. Gould, P. K. Hansma, and R. V. Coleman, J. Vac. Sci. Technol. B **9**, 1032 (1991).

[20]B. Burk, R. E. Thomson, A. Zettl, and John Clarke, Phys. Rev. Lett. **66**, 3040 (1991).

[21]R. V. Coleman, W. W. McNairy, and C. G. Slough, Phys. Rev. B **45**, 1428 (1992).

[22]B. Burk, R. E. Thomson, J. Clarke, and A. Zettl, Science **257**, 362 (1992).

[23]B. Giambattista, A. Johnson, W. W. McNairy, C. G. Slough, and R. V. Coleman, Phys. Rev. B **38**, 3545 (1988).

[24]Strictly speaking, even a uniformly incommensurate sinusoidal CDW could display "satellite" spots near each of the fundamental CDW peaks. This arises because each lattice Bragg peak will have associated with it not only first-order CDW peaks, but also a series of higher-order CDW peaks which originate from local atomic charge-density distortions due to the presence of the CDW. High-order CDW peaks associated with a given Bragg peak can appear as "satellite" spots belonging to a fundamental CDW peak tied to an adjacent Bragg peak. Calculations show, however, that such "satellites" have a very low intensity and are easily distinguished from the much more intense satellites associated with a true domain structure. For a more complete discussion of this subtle point, see B. Burk, Ph.D. thesis, University of California, Berkeley, 1994.

[25]Reference 16 concludes that the CDW maxima are identical and are at an angle of 13.9° inside the domains, while Refs. 14 and 17 conclude that the maxima are not identical and Refs. 14 and 18 measure the angle of the CDW from the real-space images at room temperature to be around 12° inside the domains.

[26]J. Schneir and P. K. Hansma, Langmuir **3**, 1025 (1987).

[27]R. E. Thomson, Ph.D thesis, University of California, Berkeley, 1991.

[28]J. A. Wilson, F. J. DiSalvo, and S. Mahajan, Adv. Phys. **24**, 117 (1975).

[29]H. A. Mizes, S. Park, and W. A. Harrison, Phys. Rev. B **36**, 4491 (1987).

[30]R. J. Colton, S. M. Baker, R. J. Driscoll, M. G. Youngquist, J. D. Baldeschwieler, and W. J. Kaiser, J. Vac. Sci. Technol. A **6**, 349 (1988); T. Tiedje, J. Varon, H. Deckman, and J. Stokes, *ibid.* **6**, 372 (1988).

[31]The reader may be curious about the appropriateness of the choice of a lattice constant as the offset vector of the two images. This choice is justifiable for the same reasons that the choice of the graphite lattice constant was justifiable in the original work of Mizes, Park, and Harrison (Ref. 29). First of all, it produces images most like those observed in real STM data. Second, it is reasonable that a small flake of the sample material adhered to the tip and acted as the tunneling tip, thereby providing several atoms separated by the sample lattice constants.

[32]G. Raina, K. Sattler, U. Muller, N. Venkateswaren, and J. Xhie, J. Vac. Sci. Technol. B **9**, 1039 (1991).

[33]The images in Fig. 10 and the derived graphs in Fig. 11 are representative of our highest-quality images; however, significant variation exists among images from a given temperature. The measured ratio of the strongest satellite amplitude to the CDW fundamental amplitude varies from about 0.75 to 0.25. The variation of this ratio leads to a corresponding variation of the strength of the derived modulation envelopes such as those shown in Fig. 11. Multiple-tip effects are the most likely explanation of this variation. Although multiple-tip effects do not alter the distribution of the satellites, they may alter their relative intensities.

[34]J. A. Wilson, J. Phys. Condens. Matter **2**, 1683 (1990).

[35]These two figures were taken at NIST, Boulder, Colorado. The software available at NIST does not allow for the apodization of the data before Fourier transforming, so these two FT's are not as clear as the others contained in this report.

[36]B. Burk and A. Zettl, Phys. Rev. B **46**, 9817 (1992).

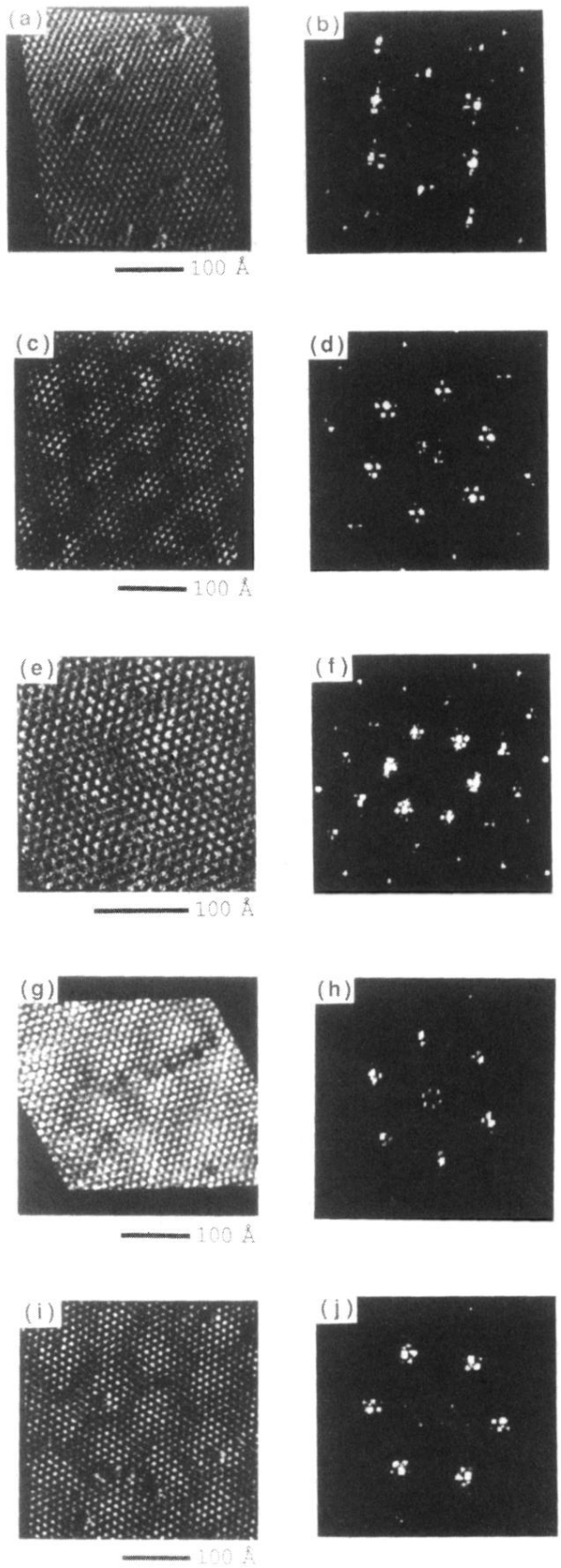

FIG. 10. (a) STM data at 343 K. (b) FT of (a). (c) STM data at 295 K. (d) FT of (c). (e) STM data at 273 K. (f) FT of (e). (g) STM data at 225 K. (h) FT of (g). (i) STM data at 215 K. (j) FT of (i). Central regions of the FT's are enlarged by a factor of 2 for better clarity of the satellite spots.

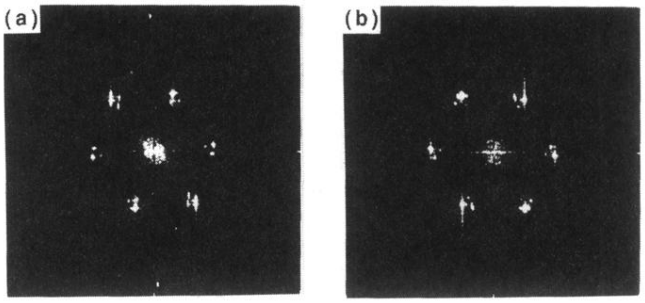

FIG. 15. (a) Fourier transform of STM data in the *NC* phase at 295 K just after the sample was cooled from the *I* phase. (b) Fourier transform of STM data of $1T$-TaS_2 in the *NC* phase at 295 K just after the sample was warmed from the *T* phase. Satellite spots are clearly visible in both FT's.

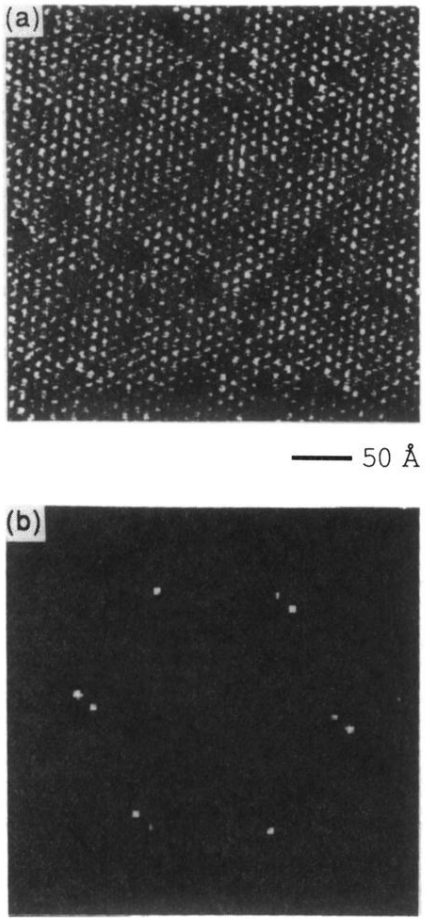

FIG. 16. (a) Real-space STM data of the T phase at 225 K. (b) Fourier transform of (a).

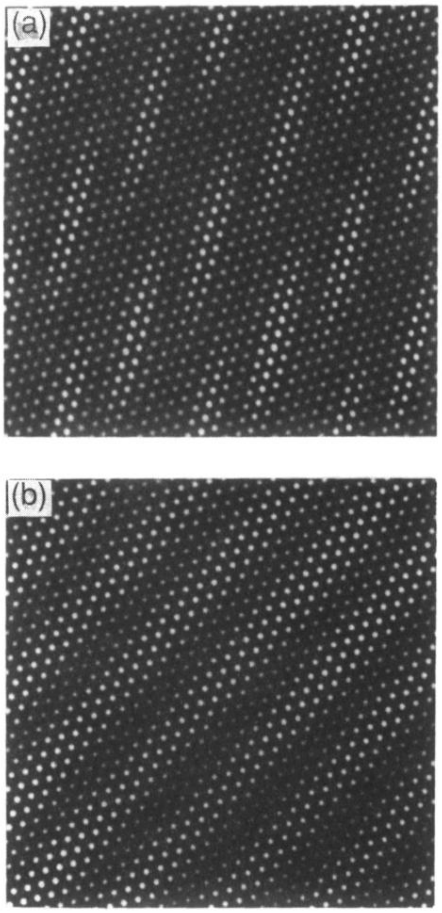

FIG. 17. (a) Computer simulation of STM data of a CDW in the stretched-honeycomb domain model of Nakanishi and Shiba (Ref. 10). (b) Computer simulation of STM data of a CDW in the striped domain model determined by Burk *et al.* (Ref. 22).

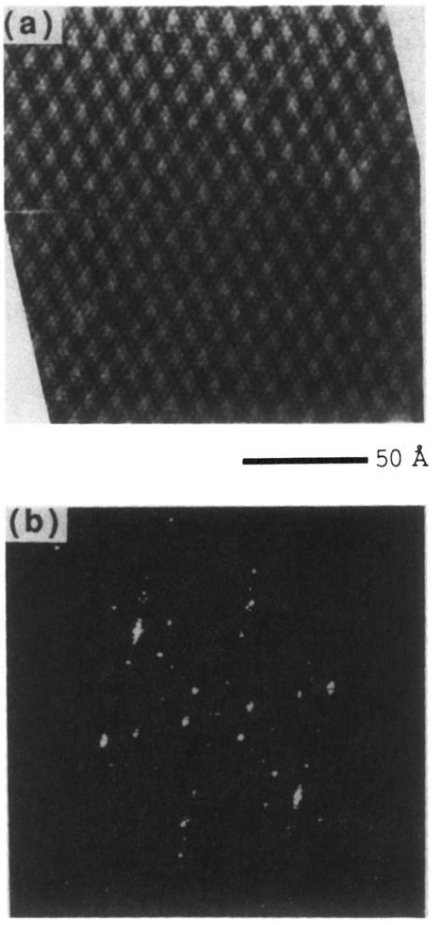

FIG. 18. (a) Real-space STM data of $1T$-TaS_2 in the I phase at 360 K. (b) Fourier transform of (a).

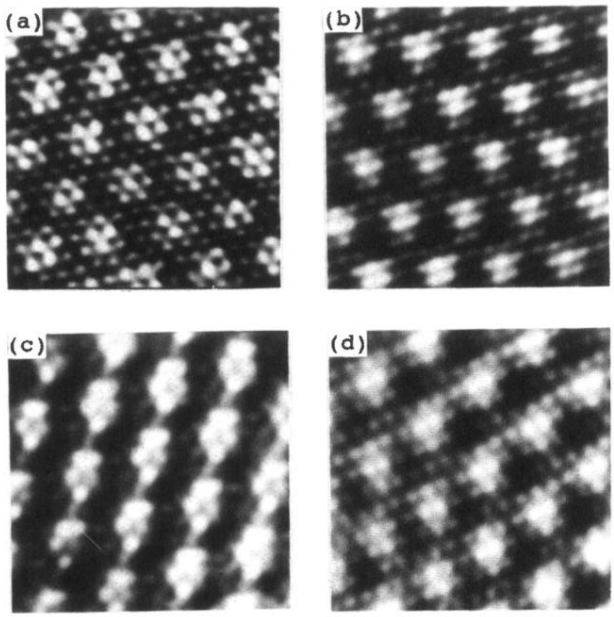

FIG. 2. Examples of high-resolution STM images, approximately 50 Å square, taken in the constant-height mode for each phase of $1T$-TaS_2. (a) *I* phase at 360 K; note that the CDW is aligned with the atomic lattice. (b) *NC* phase at 295 K; the CDW is rotated away from the atomic lattice but is not yet commensurate. (c) *C* phase at 143 K; the CDW is fully commensurate. (d) *T* phase at 236 K; similar to the *NC* phase.

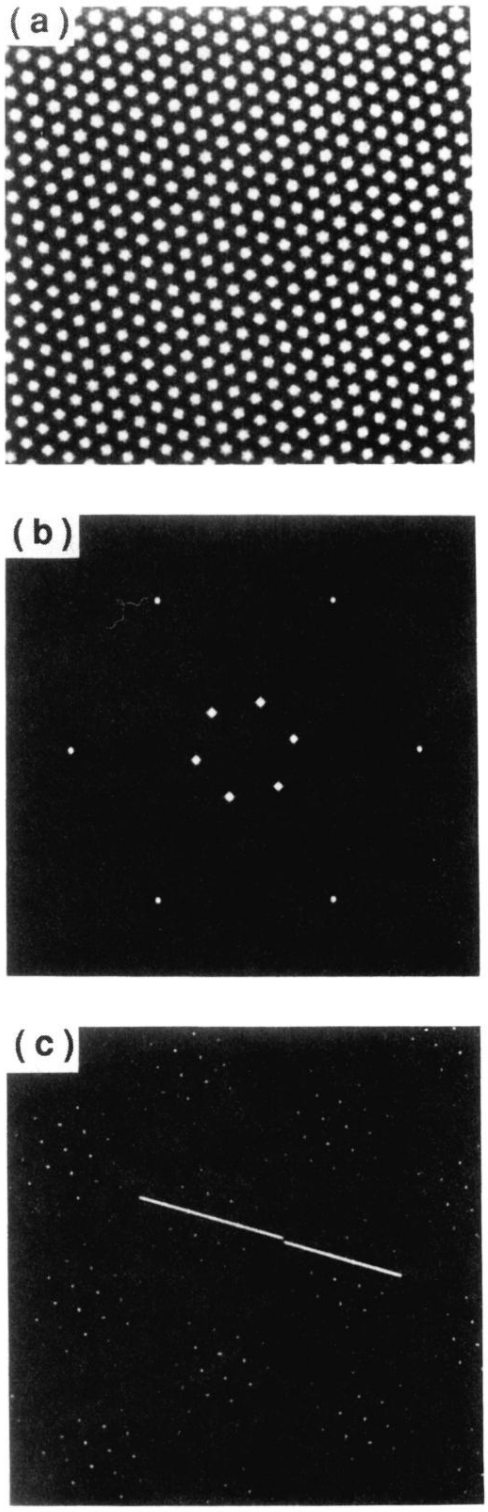

FIG. 4. Computer-generated simulation of STM images for the case where there are no domains or discommensurations in the *NC* phase. (a) Real-space image. (b) Fourier transform of (a). The six spots near the center of the transform correspond to the CDW in the real-space image, whereas the six fainter spots further from the center correspond to the atomic lattice in the real-space image. (c) Identical to (a) except that the computer gray scale has been modified to emphasize false "domains." White lines have been drawn through CDW maxima in adjacent domains to illustrate the phase shift of one lattice constant.

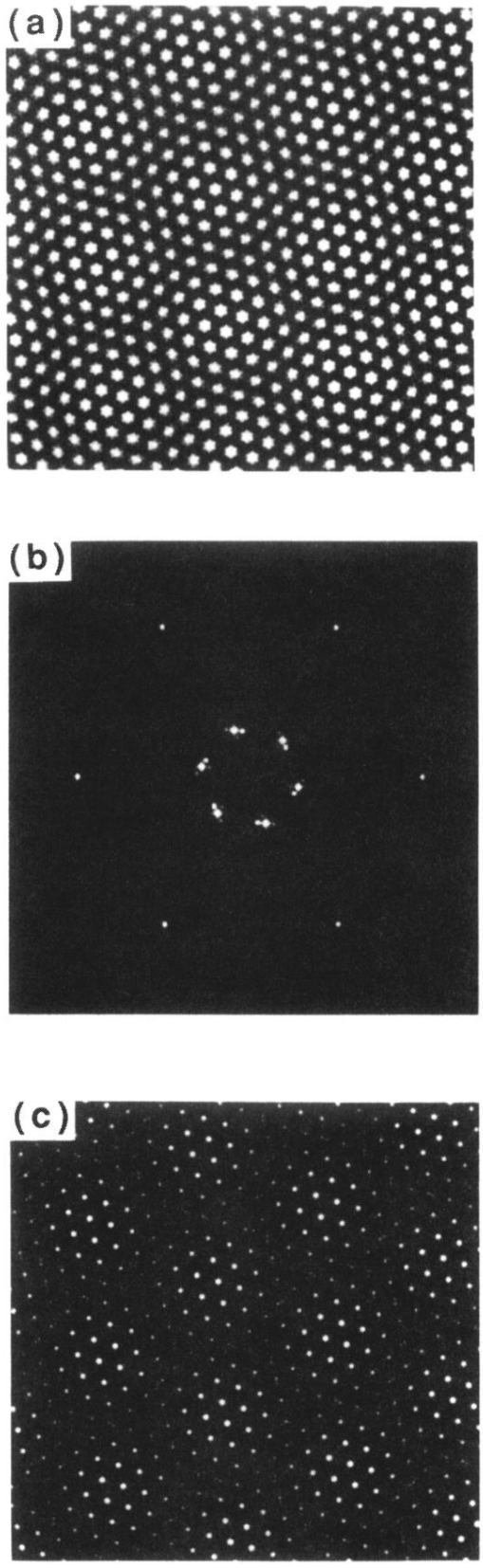

FIG. 5. Computer-generated simulation of STM images for the case where there are true domains and discommensurations in the *NC* phase. (a) Real-space image. (b) Fourier transform of (b). (c) Identical to (a) except that the computer gray scale has been modified to emphasize the domains.

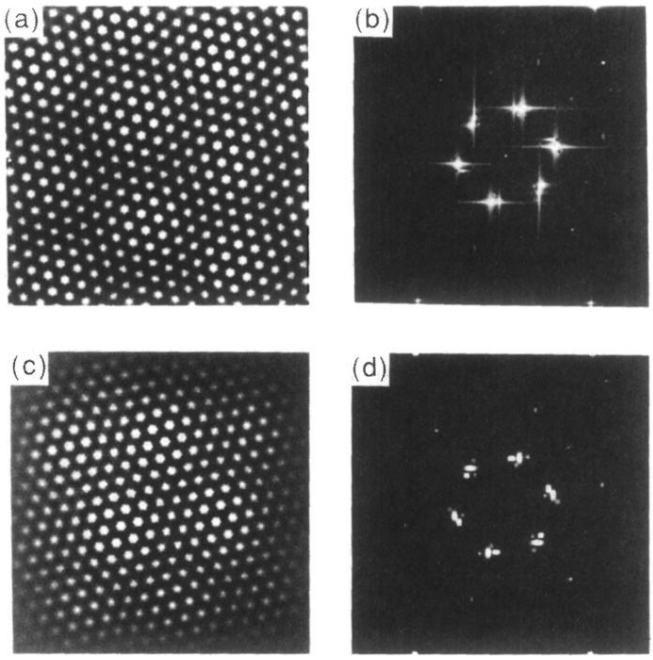

FIG. 6. (a) Computer-generated image (unapodized) of 1*T*-TaS_2 in the *NC* phase [same as Fig. 5(a)]. (b) Fourier transform of (a) showing bright streaks due to image edges. (c) Same image shown in (a) after application of the apodization filter. (d) Fourier transform of (c). Satellite spots are now more clearly visible.

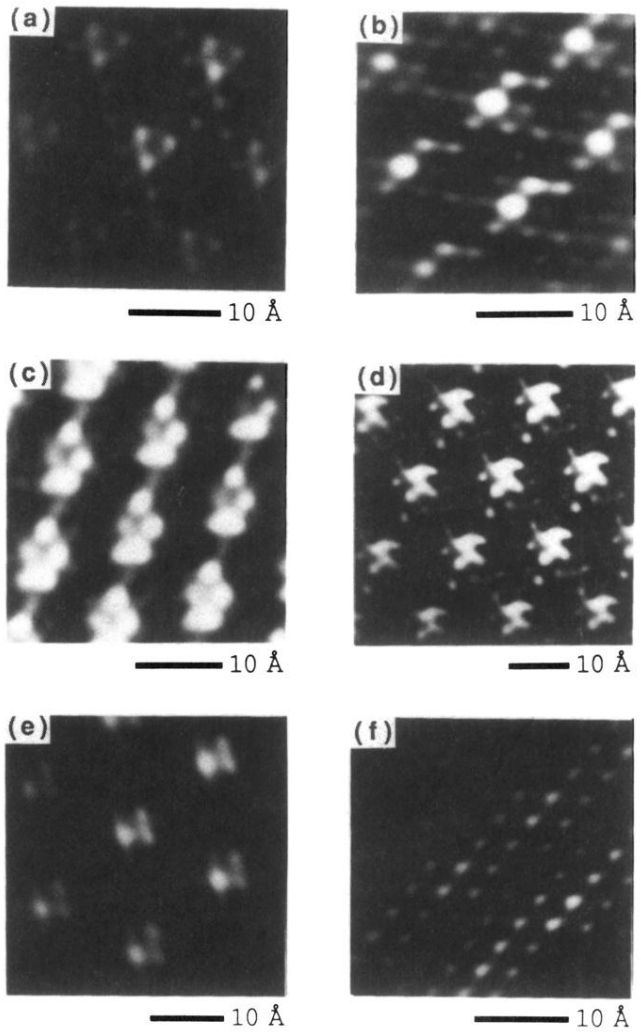

FIG. 7. Six examples of the variety of registrations we observe in STM images of the *C* phase. All images have been peak filtered (Ref. 14). (a) and (c) are in the α phase while (b), (d), (e), and (f) are in the β phase.

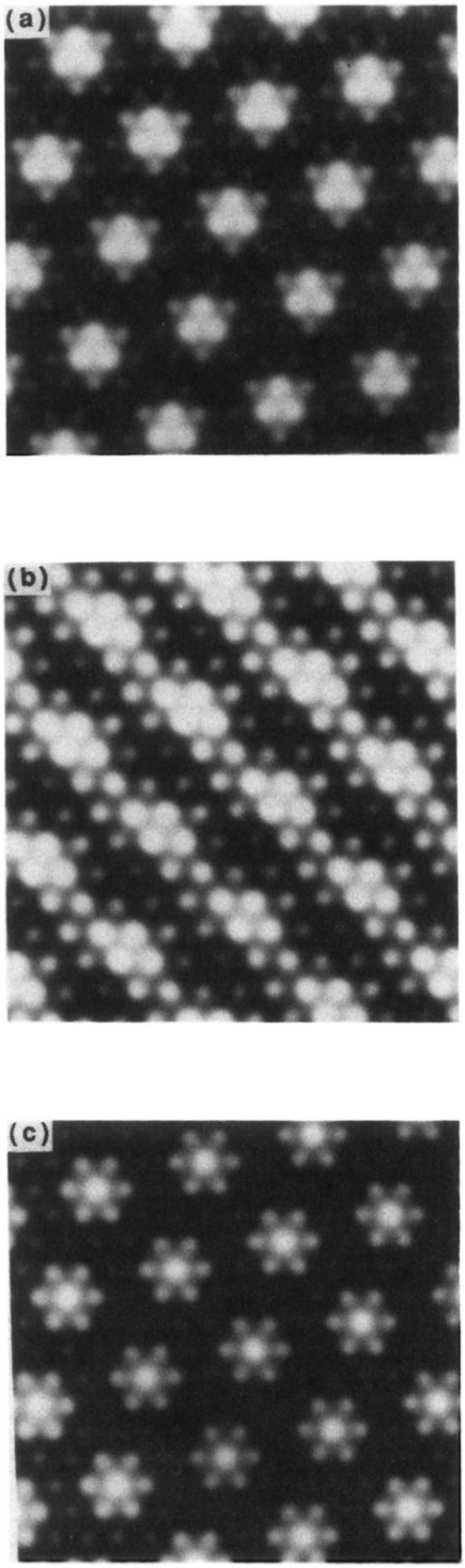

FIG. 8. Computer simulations of ideal data for the *C* phase. (a) Simulation of ideal STM data showing S atoms and the commensurate CDW. (b) Simulation of double-tip data; two images of (a) were offset from each other and added together to generate this image. (c) Simulation of triple-tip data, made by superposing three copies of (a) offset by lattice constants.

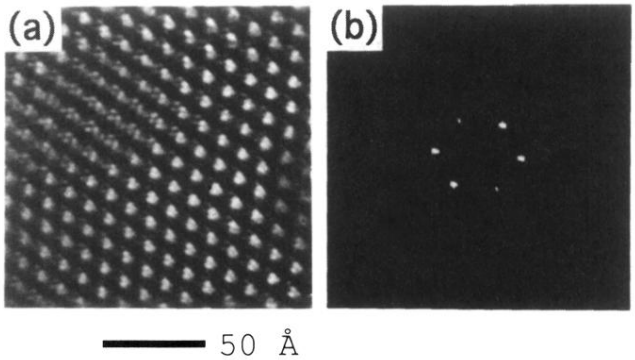

FIG. 9. (a) STM data in the *C* phase at 143 K. (b) FT of (a) with the central region enlarged by a factor of 2. Note that no satellite spots are present in the *C* phase.